

A laser-Doppler velocimetry study of ensemble-averaged characteristics of the turbulent near wake of a square cylinder

By D. A. LYN¹, S. EINAIV², W. RODI³ AND J.-H. PARK⁴

¹School of Civil Engineering, Purdue University, W. Lafayette, IN 47907, USA

²Faculty of Engineering, Tel Aviv University, Tel Aviv 69978, Israel

³Institute for Hydromechanics, Universität. Karlsruhe, D-7500 Karlsruhe, Germany

⁴Chungnam National University, Taejon, Korea

(Received 30 December 1993 and in revised form 14 July 1995)

Ensemble-averaged statistics at constant phase of the turbulent near-wake flow (Reynolds number ≈ 21400) around a square cylinder have been obtained from two-component laser-Doppler measurements. Phase was defined with reference to a signal taken from a pressure sensor located at the midpoint of a cylinder sidewall. The distinction is drawn between the near wake where the shed vortices are 'mature' and distinct and a base region where the vortices grow to maturity and are then shed. Differences in length and velocity scales and vortex celerities between the flow around a square cylinder and the more frequently studied flow around a circular cylinder are discussed. Scaling arguments based on the circulation discharged into the near wake are proposed to explain the differences. The relationship between flow topology and turbulence is also considered with vorticity saddles and streamline saddles being distinguished. While general agreement with previous studies of flow around a circular cylinder is found with regard to essential flow features in the near wake, some previously overlooked details are highlighted, e.g. the possibility of high Reynolds shear stresses in regions of peak vorticity, or asymmetries near the streamline saddle. The base region is examined in more detail than in previous studies, and vorticity saddles, zero-vorticity points, and streamline saddles are observed to differ in importance at different stages of the shedding process.

1. Introduction

The turbulent flow around a square cylinder (a definition sketch is given in figure 1*a*) has received far less attention than the flow around a circular cylinder. The topology of both flow fields is expected to be identical, but differences in length and velocity scales provide insight into the relationship between 'coherent' vortex structures and 'incoherent' (or 'random') turbulence characteristics. Features that are less apparent in the case of the circular geometry may be accentuated in the case of the square geometry. Studies of the ensemble- or phase-averaged statistics of wake flows have focused on the region, to be termed loosely the near wake, in which the individual vortex structures are clearly apparent and the turbulent vortex street is fully developed. The wake flow closer to the cylinder, within the first four diameters, has been less studied. This region, loosely termed here the base region, exhibits high levels of mixing, e.g. $\approx 60\%$ of the circulation discharged into the wake on one side of the

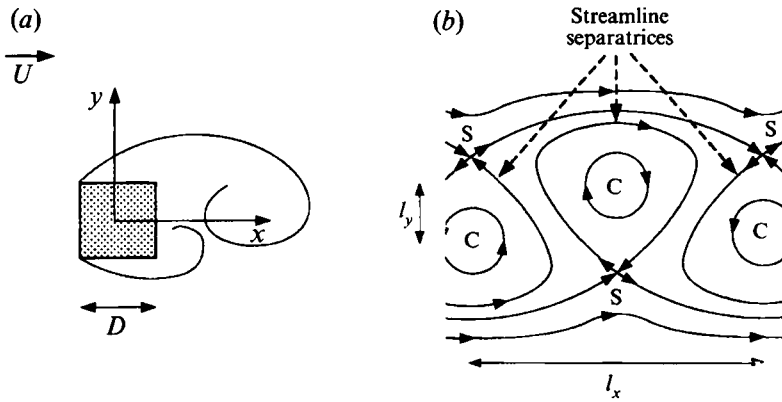


FIGURE 1. (a) Definition sketch of flow around a square cylinder, (b) sketch of streamlines of the Kármán vortex street seen from a reference frame moving with the vortices (adapted from Perry, Chong & Lim 1982): C – centres, S – saddles.

circular cylinder is lost within this region (Cantwell & Coles 1983, hereafter to be referred to as CC). In contrast to the flow pattern in the near wake, which changes little with phase except for a downstream translation, the flow in the base region changes substantially during the shedding cycle. Even if the dynamics of the base region differ from those in the near wake, a study of the former region may still provide information complementary to a study of the latter, since this region bridges the region of initial turbulent shear layer development, dealt with in Lyn & Rodi (1994), and the near wake.

1.1. Conceptual approaches

Because of the large-scale organized motion in the flow field around a bluff body, the time-varying component in the wake of a bluff-body flow includes a periodic component that may be distinguished from a residual ‘random’ (‘turbulent’ or ‘incoherent’) component. The velocity signal is appropriately analysed in terms of the triple decomposition of Hussain & Reynolds (1970), where the instantaneous streamwise velocity is decomposed as

$$u(t) = \langle u(\phi(t)) \rangle + u'(t), \quad (1a)$$

$$= \bar{u} + \tilde{u} + u'(t), \quad (1b)$$

in which $\langle u(\phi(t)) \rangle$ is the coherent component computed from the average at constant phase, $\phi(t)$ is the phase, $u'(t)$ is the turbulent component, \bar{u} is the (global) long-time-averaged velocity, and \tilde{u} is the periodic component with zero mean. Hussain (1983) gave the relevant flow equations for both coherent and turbulent flow quantities.

Critical-point theory has been exploited in discussions of separated flow patterns and of flows around bluff bodies (Perry & Fairlie 1974; CC; Perry & Steiner 1987; Zhou & Antonia 1994). For two-dimensional flows (to which this work is restricted), two non-degenerate critical (zero velocity or stagnation) points may develop in the interior of the flow field: (i) centres, characterized by closed streamlines, and (ii) saddles, characterized by the intersection of streamlines. This distinction may also be formulated in terms of the local extrema and saddle points of the appropriate stream-function distribution (see the Appendix). These will be termed here streamline centres and streamline saddles respectively. Critical points so defined are not Galilean invariant because they depend on an assumed reference frame velocity. A sketch of

critical points in an idealized Kármán vortex street consisting of point vortices all moving rectilinearly with the same velocity is shown in figure 1(b). Hussain (1983, 1986) and Hussain & Hayakawa (1987, hereafter referred to as HH) argued for the perspective of the phase-averaged vorticity distribution, $\langle \omega(x, y) \rangle$. The saddle point of $\langle \omega(x, y) \rangle$ (termed vorticity saddle), at which $\langle \omega(x, y) \rangle$ attains both a local minimum and a local maximum simultaneously, was emphasized but was used interchangeably with the streamline saddle. The vorticity saddle is based directly on a physical transported quantity and does not depend on a choice of reference frame velocity. CC suggested that a streamline saddle could be identified as a point at which $\langle \omega \rangle = 0$, and Hussain (1983, 1986) assumed that a vorticity saddle was characterized by negligible $\langle \omega \rangle$.

Besides characterizing flow patterns, critical points seem to be intimately related to turbulence (CC; HH; Kiya & Matsumura 1987) and the kinematics of mixing in general (Ottino 1989). Previous studies (CC; Perry & Steiner 1987; HH) have pointed out the importance of flow topology for turbulence quantities. Streamline centres were identified as local maxima of vorticity, and were associated with local maxima in Reynolds normal stresses or turbulent kinetic energy, $\langle k \rangle$. Streamline saddles were associated with high Reynolds shear stresses, $\langle -u'v' \rangle$, and high rates of turbulence production, $\langle P \rangle$. A model of the plane turbulent near wake that has achieved some consensus (CC; HH; Kiya & Matsumura 1987; Perry & Steiner 1987) is based on the crucial role of centres and saddles. Turbulence is produced by vortex stretching in the (streamline or vorticity) saddle region, resulting in high levels of $\langle P \rangle$ and $\langle -u'v' \rangle$ there, and is then convected along the diverging separatrix towards the streamline centre, which consequently is associated with high $\langle k \rangle$. Examination of the data for the circular cylinder of CC shows however that regions of large normal and shear stresses may overlap, and that local maxima in $\langle P \rangle$ may not all be identified with streamline or vorticity saddles.

1.2. *Previous experimental approaches*

Several techniques have been used in near-wake studies: flying-hot-wire anemometry (FHWA) (CC; Perry & Steiner 1987), laser-Doppler velocimetry (LDV) (Owens & Johnson 1980; McKillop & Durst 1986; Durao, Heitor & Pereira 1986, 1988), and particle image velocimetry (PIV) (Oshima & Ramaprian, 1991). Table 1 gives a selective summary of some recent work. The PIV study was intended mainly to illustrate the feasibility of the technique, and, while the density of velocity vectors obtained was high, the spatial resolution of the point measurement and/or the Reynolds number were low. Of the above, only Durao *et al.* (1986, 1988) dealt specifically with the square cylinder, but they did not obtain phase-averaged flow characteristics.

Of those in table 1, only the FHWA studies of CC and Perry & Steiner (1987) have reported phase-averaged statistics over any extensive region of the near wake. Phase-averaging in both studies was based on a reference signal, either a pressure or a velocity signal, at a single point. Such a reference phase becomes less relevant at distances far from the location of the reference signal, leading to contamination of the phase-averaged statistics by phase jitter (HH). Both CC and Perry & Steiner (1987) restricted measurements to within eight diameters downstream of the cylinder or normal plate. HH, in a study of the intermediate wake 20 diameters downstream of a circular cylinder, developed an iterative pattern recognition scheme, based on maximizing the correlation of the instantaneous vorticity. The vorticity was estimated by applying Taylor's hypothesis to signals from a rake of hot wires. Because the phase

Parameter	Square cylinder		Circular cylinder		Normal plate		
	Present	D88 ¹	CC ²	HH ³	MD ⁴	PS ⁵	KM ⁶
Re ($\times 10^3$)	21.4	14	140	13	15	20	23
Free-stream turbulence level (%)	2	6	0.6	n.a.	2	n.a.	0.2
Blockage (%)	7	13	4	6	10	25	7
Aspect ratio	9.75	6	29	32	10.5	9.4	15
Strouhal number	0.13	0.13	0.18	0.21	0.19	0.17	0.15
Measurement method	LDV	LDV	FHWA	HWA	LDV	FHWA	HWA
Measurement region	$-0.5 \leq x \leq 8$	$-0.5 \leq x \leq 6$	$0 \leq x \leq 8$	$x = 10, 20, 40$	$0 \leq x \leq 5$	$0 \leq x \leq 4$	$x = 8$
	$0 \leq y \leq 2.5$	$-2 \leq y \leq 2$	$0 \leq y \leq 2.5$	$0 \leq y \leq 2$	$0 \leq y \leq 1.5$	$0 \leq y \leq 1.5$	$0 \leq y \leq 3$

¹ Durao *et al.* (1986, 1988): time-averaged and band-reject filtered statistics
² Cantwell & Coles (1983): phase-averaged statistics, 16 phase bins with 1024 points per bin, reference source – pressure signal from cylinder sidewall
³ Hussain & Hayakawa (1987): rake of 8 hot wires (vertical separation, $\Delta y = 0.37$) at a single streamwise location ($x \geq 10$), phase-averaged statistics using Taylor's hypothesis and iterative correlation maximizing algorithm
⁴ McKillop & Durst (1986): only time-averaged statistics
⁵ Perry & Steiner (1987): phase-averaged statistics, 16 phase bins with 50 points per bin, reference source – stationary hot-wire signal from outside the wake
⁶ Kiya and Matsumura (1987): phase-averaged statistics by conditional averaging, reference source: hot-wire v -signal at centreline

TABLE 1. Experimental parameters

reference is local, phase jitter due to a separation distance between reference and measurement points can be reduced, but requires multipoint simultaneous measurements. A similar, though less sophisticated, conditional averaging technique was used by Kiya & Matsumura (1988) in their hot-wire anemometry (HWA) measurements eight diameters downstream of a normal flat plate. Since techniques relying on Taylor's hypothesis assume a frozen structure, they are inappropriate for any extensive flow region with significant streamwise variation such as the near-wake region.

1.3. Scope of the present work

The present work reports on an LDV study, in which the mean, the periodic, and the random component of the flow around a square cylinder at a Reynolds number of 21400 were obtained from averaging at constant phase. With its directional sensitivity, the LDV was considered essential for reliable measurements in the highly turbulent base region with instantaneous flow reversals. As a single-point technique, however, a local phase reference could not be used, so a technique similar to that of CC and Steiner & Perry (1987) was adopted for defining a reference phase. Because only a limited number of phases were used, only the largest scales corresponding to the shedding and shed vortices were resolved. The 'random' component may be alternatively viewed as a residual, analogous to subgrid scales in large-eddy simulation. The quantitative differences in length and velocity scales and qualitative similarities between the phased-averaged flow characteristics of the flow around circular and square cylinders were investigated. Asymmetries in the near wake are pointed out, and their implications for proposed models are discussed. Special interest is directed at the base region, and the relation between, on the one hand, the vorticity saddle and streamline saddle, which can be more clearly distinguished in the base region, and, on the other hand, the turbulence characteristics are examined. Only a selected portion of the large quantity of experimental data can be presented here; the complete data set is available from either the first or third author.

2. Experimental conditions and technique

The experiments were performed in a closed water channel supplied by a constant-head tank. At the measurement station, the channel had a 39 cm × 56 cm cross-section (cf. a cylinder diameter of $D = 4$ cm). The origin of the coordinate system used in the following is located in the centre of the cylinder, and all distances are non-dimensionalized by D (figure 1a). A reference velocity, U , was computed from time-averaged velocity profiles (range: $y = -4$ to $y = 4$) at several streamwise sections in the wake to be $U = 0.535 \text{ m s}^{-1}$. This is estimated to be within 2%–3% of the average cross-sectional velocity. Unless otherwise specified, all velocity quantities are non-dimensionalized with U . The Reynolds number, based on U and D , was $Re = 21400$. The shedding frequency, f , was estimated as $1.77 \pm 0.05 \text{ Hz}$ from a direct analysis of the low-pass-filtered pressure signal with the peak-finding algorithm used in the phase-sorting procedure (see below). This estimate agreed within experimental error with an estimate based on spectral analysis of the raw pressure signal. The resulting Strouhal number, $St \equiv fD/U = 0.132 \pm 0.004$ agrees with the study of Durao *et al.* (1986, 1988). Relevant experimental parameters are summarized in table 1 for the present study as well as Durao *et al.* and several other notable studies.

The \bar{u}^t -profile at $x = -3$ indicated a measureable upstream effect, with a difference between the free-stream and centreline velocity ($\bar{u}_\infty^t - \bar{u}_0^t$) of almost 0.1. This contrasts

with the results of Durao *et al.* (1986, 1988), who reported a uniform velocity profile at $x = -2.5$. Because of blockage effects, the 'undisturbed' free-stream velocity in the region behind the cylinder was actually larger than 1, namely, $\bar{u}_\infty^t = 1.1$. The free-stream turbulence level, measured upstream of the cylinder, was $\bar{u}^t \approx 0.02$; possible effects of the free-stream turbulence on time-averaged fields are discussed below in a comparison with the results of Durao *et al.* (1986, 1988).

The basic experimental technique has been described in detail by Lyn & Rodi (1994), and will only be briefly outlined. A two-colour LDV forward-scatter system measured two components of instantaneous point velocities. A reference phase was defined from a low-pass-filtered pressure signal taken from a tap at the midpoint of a cylinder sidewall. The time of occurrence of an LDV velocity realization was marked in relation to the pressure signal, permitting the association of the velocity data with a particular phase of the vortex shedding cycle. All velocity realizations occurring within the same phase bin or interval constituted an ensemble at constant phase, such that statistics at constant phase could be evaluated. A total of 20 phase bins (cf. 16 bins of CC and of Perry & Steiner 1987) was used, which, for a cycle period of 565 ms, implied a bin width of 28 ms. Because of slow data transfer and computer evaluation of the Doppler signal, the LDV signal processing system had a dead time of ≈ 100 ms, such that successive velocity realizations were necessarily placed in different phase bins and therefore different ensembles. As a result, the ensemble averages should be free of McLaughlin-Tiederman LDV bias. The number of samples in a bin varied depending on measurement point location, with a maximum of 400 samples (cf. 1024 samples in CC and 50 samples in Perry & Steiner 1987) per phase bin in the region directly behind the cylinder. The duration of a measurement at a point was generally of the order of 1 hr (at some problem points such as in the recirculation region or at points where the optical quality of the glass window was inferior, it could be several hours), or, in terms of shedding cycles, of $O(10^4)$ cycles.

Measurements were confined to the upper half of the flow region in order to reduce the number of measurements needed. It was assumed that the flow in the lower half could be obtained by reflecting the measured upper flow about the centreline. The streamwise measurement grid began at the leading edge of the cylinder and extended to $x = 8$, and included an 'inlet' profile at $x = -3$. In the lateral direction, the grid extended from the centreline to $y = 2$ in the immediate vicinity of the cylinder, and to $y = 2.5$ further downstream, as well as selected points on the streamwise grid at $y = 4$. In the region, $x < 3$, $y < 1.5$, the grid size was 0.125, but outside this region, this was increased to 0.25 or more. Within 1 cm of the cylinder, optical access by the four-beam LDV system could not be maintained, so that two-component measurements were not performed in this region. One-component measurements were obtained however in one sidewall region and were reported in Lyn & Rodi (1994).

Several checks on consistency were made on the data to provide an indication of their quality, and are discussed in more detail in Lyn (1992). The integrated flow discharge from $y = -4$ to $y = 4$ remained constant in the wake region to within 2% for both the time-averaged *and* for each of the phase-averaged fields. At $x = 8$, the time-averaged drag coefficient was estimated from the integral of the time-averaged streamwise momentum flux to be ≈ 2.1 , which agrees with accepted literature values. For a symmetric time-averaged two-dimensional field, both \bar{v}^t and $-\bar{u}^t v^t$ should vanish on the centreline. The average over all measured centreline points for \bar{v}^t was -0.04 , and for $-\bar{u}^t v^t$ was -0.007 . These may be compared with maximum absolute values of \bar{v}^t and $-\bar{u}^t v^t$ which exceeded 0.3 and 0.1 respectively. These comparisons give some

support to the two-dimensionality achieved in the flow. The validity of the reflection procedure was examined by considering the centreline measurements of the ensemble-averaged fields, since the reflection procedure results in an additional measurement at each centreline point. The average magnitude of the difference between the original and the reflected ensemble-averaged measurements on the centreline for $\langle u \rangle$, $\langle v \rangle$, and $\langle -u'v' \rangle$ was typically 0.01, 0.07, and 0.006. (In figure 5a below, two estimates of the velocity vectors on the centreline based on the reflection assumption are shown.) From these checks, the uncertainty in the ensemble-averaged results for $\langle u \rangle$, $\langle v \rangle$, $\langle u' \rangle$, $\langle v' \rangle$ is estimated to be less than 0.05, with the largest uncertainty in $\langle v \rangle$. In terms of the profile maximum, the uncertainty in $\langle -u'v' \rangle$ is expected to lie in the range 15% – 25% in the region of large profile maxima, e.g. in the base region, but may be larger further downstream as the profile maxima in $\langle -u'v' \rangle$ decrease. The uncertainty in quantities based on estimates of velocity gradients may be substantial. Estimates of local divergences ($\partial \langle u \rangle / \partial x + \partial \langle v \rangle / \partial y$) could attain magnitudes of 1 or more at isolated points. In the contour plots to be presented of quantities involving velocity gradients, points at which the estimates of absolute local divergence were larger than 0.4 were excluded; these typically represented less than 10% of the total measurement points.

In the following, contour plots of various fields will be important in the discussion of flow topology, since identification of centres and saddles and extremal features is based on visual examination of the appropriate contours. The contours were generated (with routines from the NCAR software package) from unfiltered raw data, but smoothing was applied. Hence, the location of flow features, such as centres and saddles as given in the following, while considered to be relatively reliable, should be viewed with some caution. It may also be argued that the errors introduced by the contour plotting are random rather than systematic. As the ensemble-averaged features seen in the limited results presented here are typical of all phases, the discussion based on them is not necessarily very sensitive to contouring imperfections.

3. Experimental results

3.1. *The mean (long-time-averaged) field*

For an unsteady flow, the mean flow is an artificial construct, but it remains useful as an analytical tool as a base flow over which is superimposed the motion of vortex structures. It also affords a comparison with the only other published velocity results on the flow around a square cylinder (Duraó *et al.* 1986, 1988). The mean field may also play a more important role according to recent theoretical work on the absolute stability of the mean velocity profile in the near wake (Triantafyllou, Triantafyllou & Chrysostomidis 1986).

The streamwise variation of several mean centreline quantities is compared in figure 2 with published results for both circular and square geometries. The present results for centreline velocity, $\bar{u}_0 = \bar{u}(x, 0)$, agree with those of Duraó *et al.* (1986, 1988) for $x \leq 3$. The mean recirculation region extends to $x = 1.4$, compared to, for the circular cylinder, a recirculation length of 1 (CC) at relatively high Re , and 1.65 (McKillop & Durst 1986) at an Re closer to the present work. A coordinate system with origin at the cylinder centre may however not be the most appropriate for comparing the size of the recirculation region in the two geometries since the streamwise coordinate of the separation point differs (but see the discussion of lengthscales in §4.2). In both geometries, the mean fields in the base region are

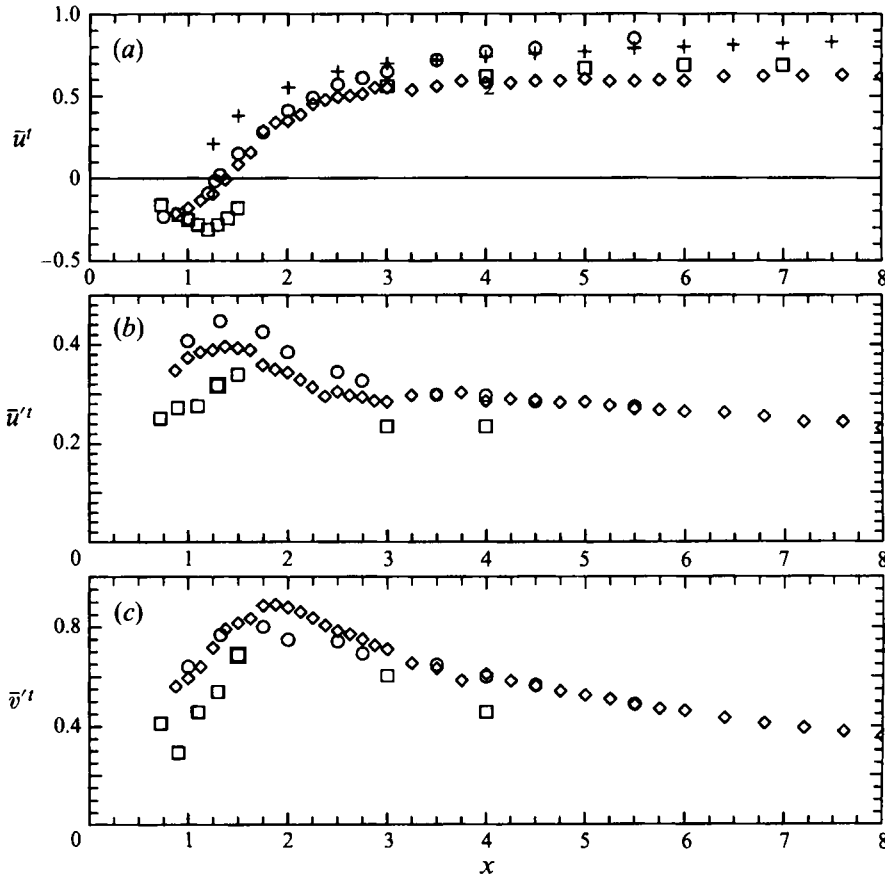


FIGURE 2. Comparison of time-averaged results for streamwise variation: \diamond , present results; \circ , Durao *et al.* (1986); +, CC; \square , McKillop & Durst 1986. (a) Centreline velocities, (b) root mean square of horizontal velocity fluctuations, and (c) root mean square of lateral velocity fluctuations.

characterized by relatively rapid streamwise variations; farther downstream, the mean flow varies much more slowly. For $x > 3$, the present results differ significantly from those of Durao *et al.* (1986). Because the wake is wider for the square than for the circular cylinder, mean centreline velocity recovery in the former is expected to be slower than the latter, as is the case in figure 2. Differences between the two circular cylinder cases, attributed by McKillop & Durst (1986) to differences in Re , are also quite substantial. For the present case of sharp-edged bluff bodies, the effect of different Re is expected to be much less dramatic.

The present results for \bar{u}^t and \bar{v}^t on the centreline agree well with Durao *et al.* (1986) in the near wake. In the base region, the present results indicate a lower \bar{u}^t and a higher \bar{v}^t for $x < 3$. Both the present results and Durao *et al.* (1986, 1988) show however that \bar{u}^t and \bar{v}^t for the square cylinder case are larger than those for circular cylinder case, with \bar{v}^t attaining a maximum of ≈ 0.9 . The difference between the near wake ($x > 4$) and the base region $x < 4$ is also seen in the much larger streamwise changes in the latter. The profiles of various mean quantities at $x = 1$ are compared in figure 3 with the results of Durao *et al.* (1986) and those of CC. Durao *et al.* (1986) took measurements in both upper and lower halves of the flow, so their results have been reflected about the centreline, with measurements in the

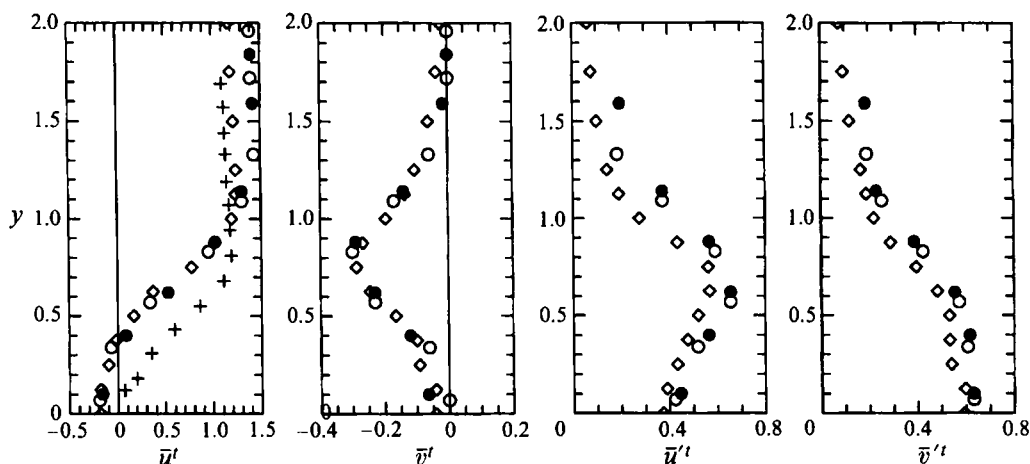


FIGURE 3. Comparison of time-averaged profiles of \bar{u}^t , \bar{v}^t , u' , and v' at $x = 1$: \diamond , present results; \circ , Durao *et al.* 1986 (one side); \bullet , Durao *et al.* 1986 (the other side reflected); $+$, CC.

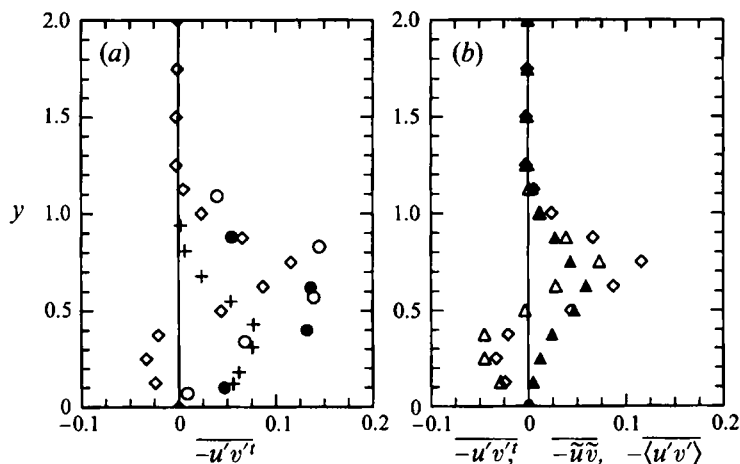


FIGURE 4. Comparison of time-averaged profiles of $-\bar{u}'v'^t$ at $x = 1$: (a) with previous measurements (symbols as in figure 3), (b) with contribution due to periodic component, Δ , and due to turbulent component, \blacktriangle .

two halves being distinguished. Good agreement is found in both \bar{u}^t - and \bar{v}^t -profiles. The square-cylinder wake is $\approx 25\%$ wider than the circular-cylinder wake. The data of CC may not be comparable because of the much larger Re , but the data of McKillop & Durst (1986) at a more comparable Re but at a slightly different x show a similar trend. The effects of blockage are more marked in the square case, and so \bar{u}^t is significantly larger than unity in the free-stream (in Durao *et al.* 1986, with the largest blockage, almost as large as 1.5). The agreement of \bar{u}^t - and \bar{v}^t -profiles is generally good, except that the results of Durao *et al.* (1986) tend to be systematically larger than the present results, particularly towards the free stream.

The $-\bar{u}'v'^t$ -profile (figure 4a) exhibits two extrema, an expected maximum in the shear layer region, and an additional local minimum of opposite sign nearer the centreline within the recirculation region. Although the latter feature does not appear in Durao *et al.* (1986), a similar feature is clearly observed in the circular-cylinder

data of McKillop & Durst (1986) at a slightly different streamwise location. It is not seen in the data of CC at $x = 1$ since this section occurs at the end of the recirculation region for their case. The periodic and the random components of $-\overline{u'v'}$ are presented separately in figure 4b. The latter, $\overline{\langle -u'v' \rangle}$, i.e. the average over all phases of $\langle -u'v' \rangle$, shows a single maximum. Thus, the local minimum seen in $-\overline{u'v'}$ is due entirely to the periodic component, $-\overline{u\tilde{v}}$, which exhibits two extrema.

Discrepancies between the present results and those of Durao *et al.* (1986) are largely attributed to the larger blockage, smaller aspect ratio, and the higher free-stream turbulence level of the latter. West & Apelt (1982) have shown, for flow around circular cylinders, that larger blockage and smaller aspect ratios are associated with a more negative mean base pressure and hence higher drag coefficients. Higher turbulence intensities (due to small-scale turbulence) result in the opposite effects (Courchesne & Laneville 1982; Nakamura 1993). The relatively good agreement with the results of Durao *et al.* (1986) in the region $x < 3$ indicate that the opposing effects of the different experimental conditions cancel each other in the base region. Farther downstream, however, the effects may be reinforcing rather than opposing. Higher free-stream turbulence levels enhance entrainment into the wake, while larger blockage sharpens mean cross-stream velocity gradients thereby also promoting entrainment, with the final result that the centreline velocity in the experiment of Durao *et al.* (1986) recovers significantly more quickly. Such effects should also be borne in mind in the following comparisons with the circular-cylinder results of CC, though the effects of modest differences in blockage (7% compared to 4%) and in turbulence levels (2% compared to 0.6%) seem unlikely to change substantially the main results.

3.2. The velocity field and its critical points

A velocity vector plot for a single phase ((9,19), chosen since it corresponds approximately to CC's phase (7,15) for which most results were given), is shown in figure 5(a) for a reference frame fixed to the cylinder. The figure also shows the measurement grid (additional measurements at $y = 4$ and at $x = -3$ were also taken but not shown). Within a region, $x \leq 0.5$, $0.5 < |y| < 0.75$, only one-component measurements were available, so that, for the purposes of figure 5(a), the cross-stream velocity, $\langle v \rangle$, in this region was set to zero. The two estimates of the velocity vector along the centreline, arising from the reflection about the centreline, agree fairly well. In this reference frame, a centre and an associated saddle are observed for this phase immediately downstream of the cylinder at $(x, y) \approx (1.1, 0)$ and $(x, y) \approx (1.4, -0.6)$ respectively, with only a wavy structure seen farther downstream. The corresponding instantaneous streamlines are shown in figure 5(b); these were computed by integrating the $\langle u \rangle$ -field at a section across the stream, assuming an undisturbed flow at $y = -4$, taken as a zero streamline. The closed streamlines characteristic of a centre (at $(x, y) \approx (1.2, 0)$) and the (near) intersection of streamlines characteristic of a saddle (at $(x, y) \approx (1.5, -0.7)$) may be seen. This centre is *not* however associated with any vortex structure, and its physical relevance is dubious.

Streamlines are shown for two different phases in two different reference frames moving with streamwise velocities of 0.43 (figure 6a, phase (5,15)) and 0.78 (figure 6b, phase (9,19)) respectively. These velocities are based on estimates of vortex celerities discussed below. In figure 6(a), a streamline centre is observed at $(x, y) \approx (2.1, -0.2)$, and the associated streamline saddle is located at $(x, y) \approx (2.3, 0.8)$. The centre-saddle system is elongated in the cross-stream direction, and inclined with respect to the centreline, and corresponds to a vortex structure, which has not yet been completely

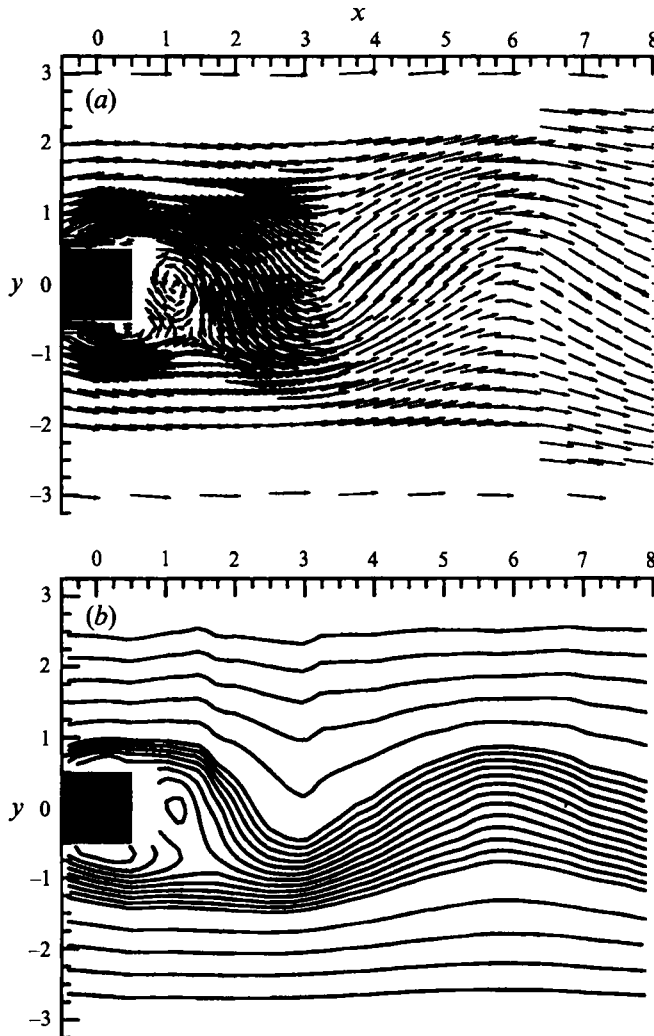


FIGURE 5. (a) Velocity-vector plot, and (b) streamline plot, at phase (9,19) in the reference frame of the cylinder (stream-function values were chosen to highlight critical points and are not equidistant).

'shed'. figure 6(b), in which at least three streamline centre-saddle systems can be observed, resembles closely the idealized sketch of figure 1(b). The centre-saddle system at $x \approx 6$ corresponds to a shed vortex structure, and exhibits greater upstream-downstream symmetry than seen in the still-attached structure of figure 6(a). With the downstream growth of the wake and the vortex structure, the distance between centre and saddle also increases.

Although each streamline centre-saddle system of figure 6(b) does correspond to a vortex structure, their locations may not be precisely determined from figure 6(b). Before, during, and after shedding, a vortex structure will move with different velocities. A single choice of a reference frame velocity can be made only for a single structure. In the near wake, vortex celerities change slowly, and so a single reference frame velocity may be useful for this region. The motion of the vorticity peak may differ from that of the centroid of the vorticity distribution (see §3.4 for a discussion of the estimation of the centroid location). The latter was selected as the basis for

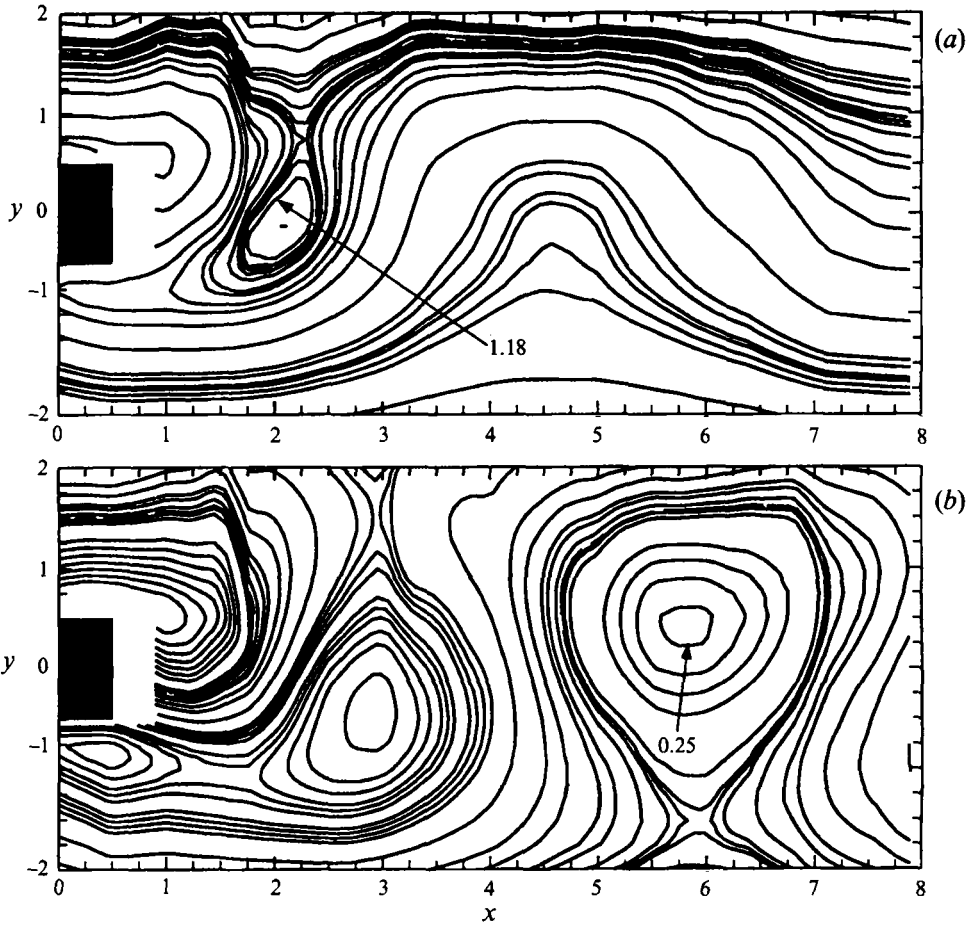


FIGURE 6. Streamline plots from reference frame moving with a selected vortex structure: (a) phase (5,15), $U_c = 0.43$, vortex structure with centre at $x \approx 2.1$; (b) phase (9,19), $U_c = 0.78$, vortex structure with centre at $x \approx 5.9$ (stream-function values were chosen to highlight critical points and are not equidistant).

determining the reference frame velocity since the location of the centroid is more reliably determined. The reference-frame velocity of 0.78 is based on the celerity of the vorticity centroids for $x > 4$, so that only the location of the centre and saddle of the structure at $x \approx 6$ can be reliably determined. Estimates of celerity of the vorticity peak tend to be $\approx 5\%$ lower than that of the vorticity centroid, but are subject to greater uncertainty. If based on the the vorticity peak, the locations of the streamline centre and saddle would be slightly shifted towards the centreline.

3.3. Vorticity centres (peaks) and saddles

Vortex structures are directly observed from contours of $\langle \omega \rangle \equiv \partial \langle v \rangle / \partial x - \partial \langle u \rangle / \partial y$ (figure 7). Gradients were computed using a three-point scheme with smoothing applied only in drawing the contours. The $\langle \omega \rangle = 0$ line is drawn but should be regarded with caution in regions of small vorticity gradients, e.g. in the near wake away from the centreline, because of uncertainties in $\langle \omega \rangle$ -estimation and limitations of the contouring software. The streamline centre seen in figure 5(b) does not correspond to any vorticity peak, and the vorticity peaks of figure 7(a) beyond $x = 3$ are not found

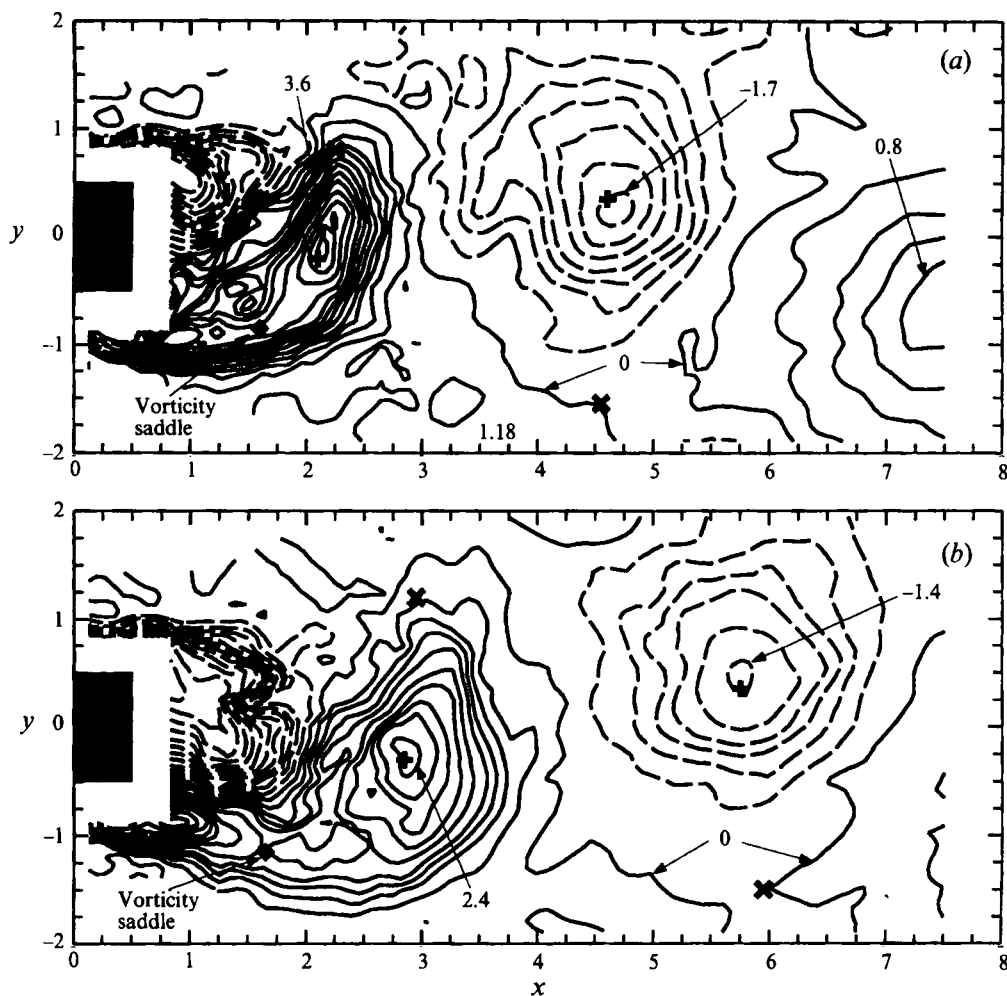


FIGURE 7. Contour plot of $\langle \omega \rangle$ for (a) phase (5,15), (b) phase (9,19): - - - - -, negative values, ———, positive values; contour intervals $|\langle \omega \rangle| \leq 0.8 : 0.2$, $0.8 \leq |\langle \omega \rangle| \leq 2.4 : 0.3$, $2.4 \leq |\langle \omega \rangle| \leq 3.6 : 0.4$. In this and following contour plots, the approximate location of some streamline centres (+) and saddles (x) as well as vorticity saddles (◆) are given.

in either figure 5(b) or figure 6(a). Also drawn on figure 7 and on subsequent contour plots are approximate locations of streamline centres and saddles in the central region $2 \leq x \leq 7$, determined from streamline plots based on estimated vortex celerities. Vortex peaks coincide within experimental uncertainty with the relevant streamline centres. Streamline saddles in the near wake similarly correspond to a zero- $\langle \omega \rangle$ point, but the zero- $\langle \omega \rangle$ -contour in the base region lies well above the streamline saddle. Vorticity saddles in the near wake are difficult to identify precisely because of the low levels of vorticity, but are close to zero- $\langle \omega \rangle$ points. Thus, vorticity and streamline saddles are indistinguishable within experimental accuracy, and are located in regions where $\langle \omega \rangle \approx 0$. In the base region, vorticity saddles are more easily identified, but their relation to streamline saddles is more complex, as further discussed in §4.3.

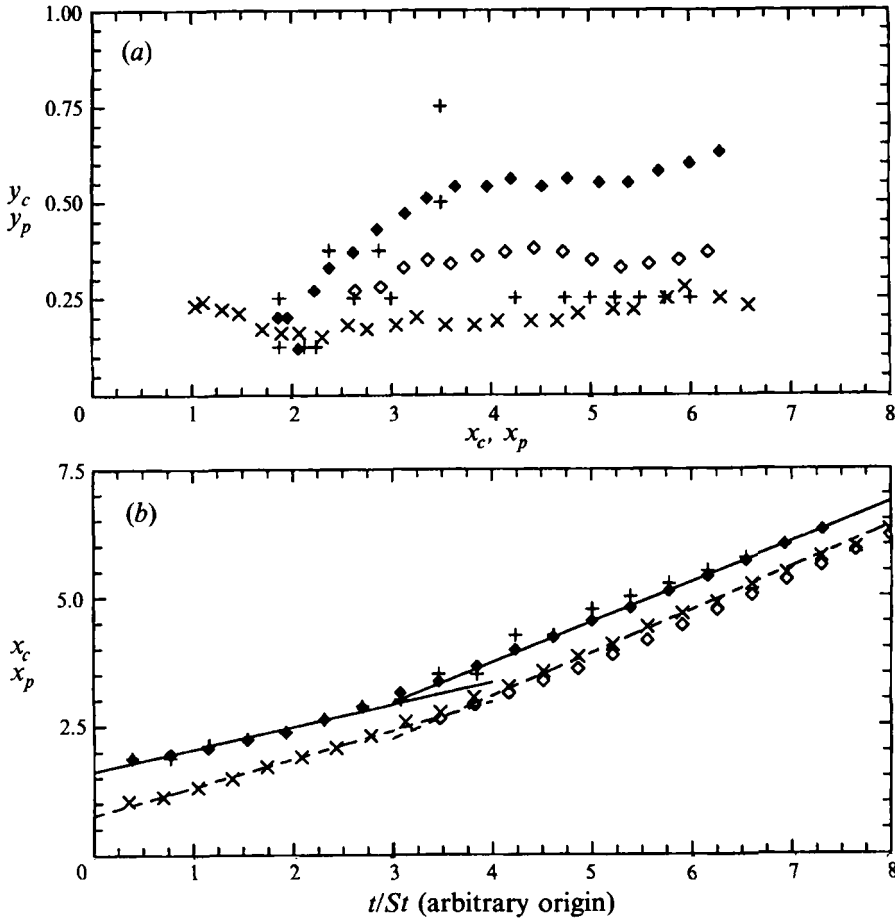


FIGURE 8. Characteristics of vortex structure motion. (a) Trajectory of vortex centroids, \blacklozenge , present results; \diamond , CC; and vortex peaks: $+$, present results; \times , CC. (b) Variation of streamwise location of vortex centroids and peaks with time or phase (symbols as in (a)): —, slope = 0.78 for $x > 4$, slope = 0.43 for $x < 3$; ----, slope = 0.83 for $x > 4$, slope = 0.55 for $x < 3$.

3.4. Vortex motion and downstream variation of vortex characteristics

The $\langle \omega \rangle$ -distribution is not circularly symmetric about the peak, and so peaks do not coincide with the centroids. The location of the peak, (x_p, y_p) , may be the more physically relevant, but its determination is complicated by noise in the data as well as coarseness of the measurement grid. A large scatter is observed in (x_p, y_p) in the base region (figure 8(a)). Being based on averaging over a large number of points and a large area, the location of the centroid, (x_c, y_c) , is determined more reliably, and hence its variation is smoother. Centroids were computed with a variable cutoff, $|\langle \omega \rangle_0|$, and a specified flow region, using

$$\xi_c = \frac{\sum_{|\langle \omega \rangle_{i,j}| \geq |\langle \omega \rangle_0|} \xi \langle \omega \rangle_{i,j} \Delta A_{i,j}}{\sum_{|\langle \omega \rangle_{i,j}| \geq |\langle \omega \rangle_0|} \langle \omega \rangle_{i,j} \Delta A_{i,j}}, \quad (2)$$

where ξ is either x or y , and $\Delta A_{i,j}$ is an element of area over which $\langle \omega \rangle_{i,j}$ is assumed to take on the measured point value. The cutoff, $|\langle \omega \rangle_0|$, was taken to be 0.05 in

the lower-vorticity near-wake region compared to maximum values of $|\langle\omega\rangle_0|$ typically greater than 1.5. A higher cutoff value of 0.15 (cf. maximum $|\langle\omega\rangle| > 3$) was applied in the base region, where vortex structures had tails with significant levels of vorticity. The specified flow region over which (2) was taken was determined from contour plots of $\langle\omega\rangle$ such as figure 7 on the basis of identifying distinct vortex structures.

Peaks for $x > 4$ are located close to the centreline, at $y_p \approx 0.25$, while centroids are located at $y_c \approx 0.55$. In this region, the measurement grid size in y , $\Delta y = 0.25$, so an uncertainty in y_p of ± 0.1 – 0.2 may be expected. For $x < 3$, $|y| < 1.5$, where $\Delta y = 0.125$ or smaller, y_c and y_p may approach each other, though y_p -values are erratic because of the scatter in the maximum values of $|\langle\omega\rangle|$. CC reported values of $y_p < 0.25$ and $y_c < 0.4$ throughout the near wake, reflecting the smaller width of the circular-cylinder wake. Towards the end of the measurement region, $x_c > 6$, a tendency for y_c and y_p to increase is observed.

The streamwise location of the vortex centroid and vortex peak as a function of a nondimensional time, t/St , is shown in figure 8(b) (this coordinate was chosen because the slope gives directly the vortex celerity). For $x_c > 4$, x_c varies approximately linearly with t/St , with a slope reflecting a constant celerity, $U_c = 0.78$, which was used previously in figure 6(b) as the velocity of the reference frame. For the circular cylinder, a value of $U_c = 0.83$ in the comparable region is inferred (CC), while for the normal bluff plate, Fage & Johansen (1927) reported a value of 0.765, and for a rectangular cylinder, Bearman & Trueman (1972) reported a value of 0.76. The small difference in U_c for the square and the circular geometries contrasts with the substantial difference in mean centreline velocity, \bar{u}_0^t (figure 2a). Both results are however correlated by $U_c = 0.45 (\bar{u}_\infty^t + \bar{u}_0^t)$, where in the present case, the measured mean free-stream velocity, $\bar{u}_\infty^t = 1.1$, was used. Celerities in a steady self-similar plane mixing layer are usually described by a similar correlation with, however, a coefficient of 0.5 rather than 0.45. This may point to an indirect relationship between vortex motion and mean velocity gradients or strain rates, in which the vorticity peak adjusts its location to maintain a stable celerity. The value, $U_c = 0.78$, is larger than the value of 0.71 for $\bar{u}^t(x_c, y_c)$, but U_c should be more closely related to $\langle u \rangle(x_p, y_p)$ (HH), and generally better agreement is obtained between U_c and $\langle u \rangle(x_p, y_p)$.

In the base region, the centroid is not well defined since the distribution is not ‘compact’; hence, the centroid as computed depends more strongly on the chosen cutoff value and the specified flow region, and (x_c, y_c) of figure 8 in this region is thus more closely related to the vortex peak. A linear variation is less clear for $x < 3$, though an average streamwise celerity, $U_c = 0.43$, may be inferred (cf. a value of 0.55 for the circular cylinder). Unlike \bar{u}_0^t in the near wake, which is only slowly varying, \bar{u}_0^t in the base region varies rapidly downstream, contrasting sharply with the relative constancy of U_c . A simple mixing-layer-type correlation based on the average of mean free-stream and centreline velocities therefore is inadequate. Nevertheless, vortex structures do develop from shear layers with both a low-velocity and a high-velocity side. Although velocities in the base region may be low, the high-velocity region of the shear layer will equally influence the celerity of vortex structures, which will therefore be significantly larger than zero. The high values of celerities imply that, in much if not all of this region, a reference frame fixed to the cylinder is not useful.

3.5. The periodic component

The variation with phase of $\langle u \rangle$ and $\langle v \rangle$ (also \bar{u} and \bar{v}) at various cross-stream points at a base-region station ($x = 2$) and at a near-wake station ($x = 6$) is shown in figure 9.

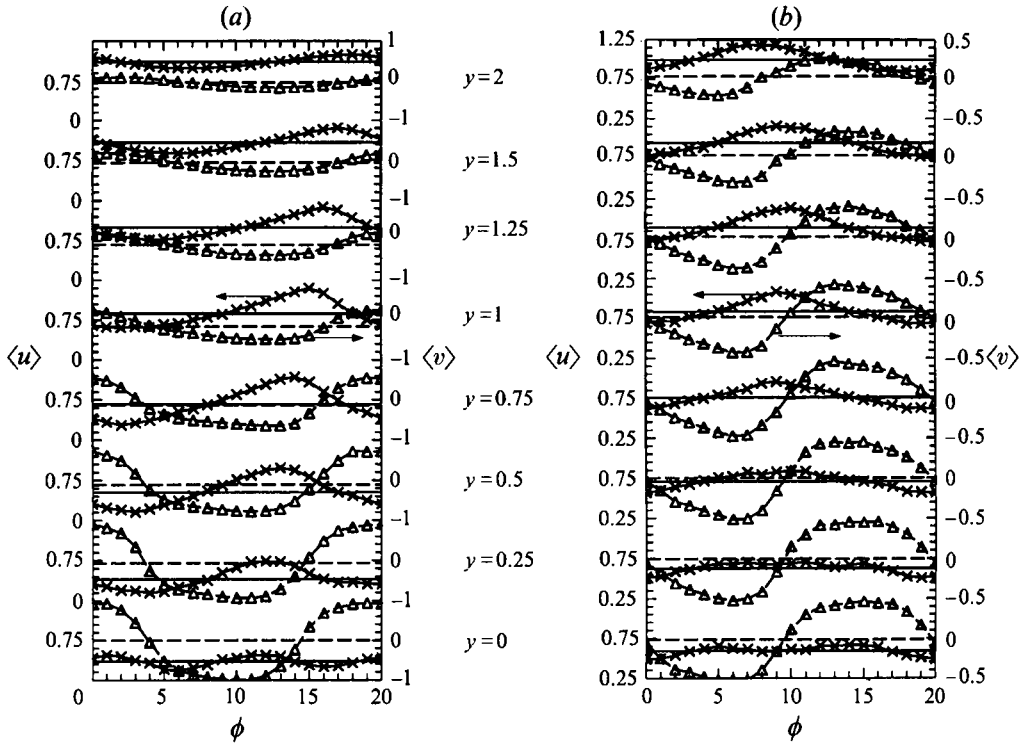


FIGURE 9. Variation with phase of $\langle u \rangle$, \times , and $\langle v \rangle$, Δ , at the same lateral locations at two sections, (a) $x = 2$ and (b) $x = 6$. Lines are drawn for visual clarity only; horizontal lines indicate average over all phases: —, $\langle u \rangle$; - - - - , $\langle v \rangle$.

The sharp decrease in \bar{u} at $x = 2$, $0.5 \leq y \leq 1$, accompanied by a sharp increase in \bar{v} , signal the shedding of a vortex structure. Near the centreline trajectory of vortex peaks, \bar{v} is quite flat for much of the cycle, this being associated with free-stream fluid being drawn across the centreline, but makes an abrupt transition as a peak of concentrated vorticity passes by. After a structure becomes well defined, vorticity peaks are located in regions where both $\bar{u}\bar{u}$ and $\bar{v}\bar{v}$ are small (figure 10). At these peaks, $\langle u \rangle \approx U_c$, such that the amplitude of \bar{u} and hence $\bar{u}\bar{u}$ is small, while values of \bar{v} and $\bar{v}\bar{v}$ at centres are small because $\langle v \rangle \approx \bar{v}^t \approx 0$. Between successive peaks, the periodic motion is primarily cross-stream, and so \bar{u} remains small along the almost horizontal trajectory of the vortices, with the result that $\bar{u}\bar{u}$ is small along the entire centreline region.

A gross symmetry about the centreline of the contours of $\bar{u}\bar{u}$ and $\bar{v}\bar{v}$ was noted by CC, but peak magnitudes of $\bar{u}\bar{u}$ on one side of the centreline may be more than 50% larger (just after shedding, up to 300%) than those on the other side at the same streamwise location. The largest magnitude of $-\bar{u}\bar{v}$ (figure 10c) associated with a structure is observed downstream of the vortex peak, on the same side of the cylinder as that on which the given vortex was shed. The magnitudes of the extrema on the other side are noticeably less, attributable to mixing occurring near the saddle region. The 'strength' of rotation is thus quite non-uniform. A wide swath of same-signed $-\bar{u}\bar{v}$ -contours extends obliquely from one side of the centre line to the other, and is believed to be associated with anomalous features in the distribution of the Reynolds shear stress, $\langle -u'v' \rangle$, as discussed below.

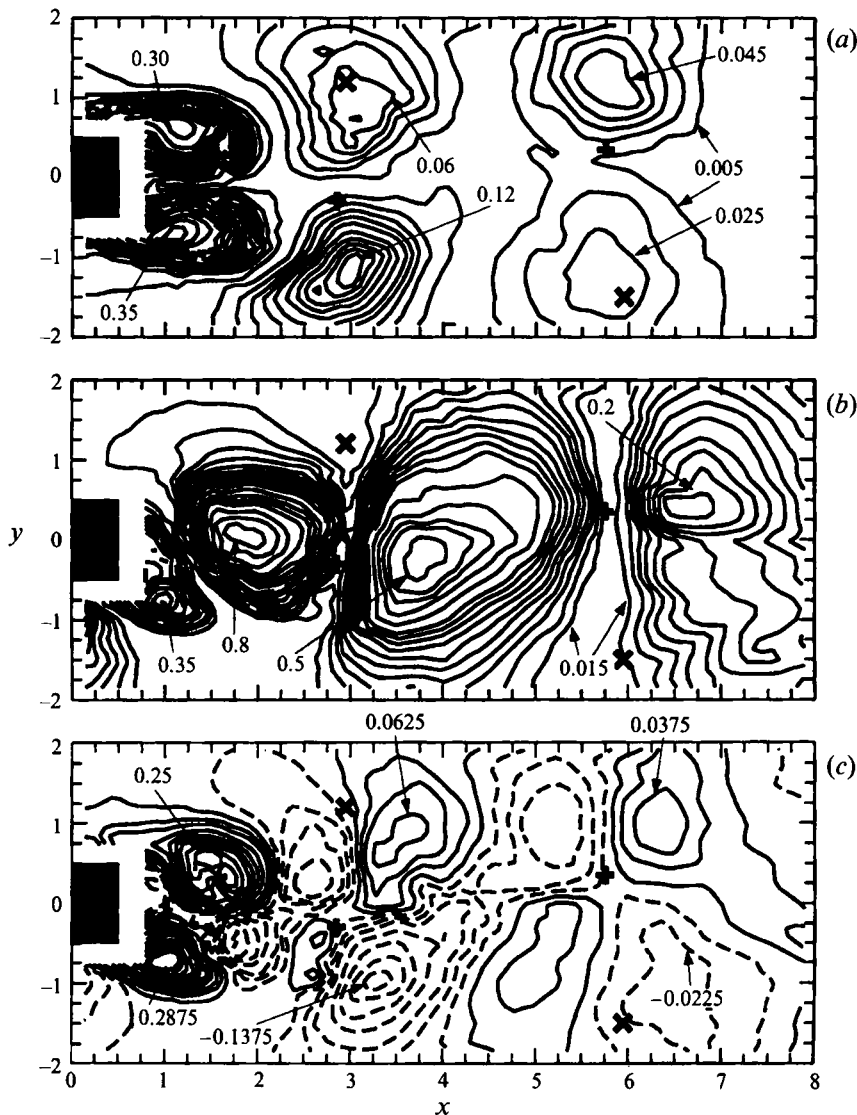


FIGURE 10. Contour plots of the periodic stresses for phase (9,19): (a) $\bar{u}'u'$, minimum value contour -0.005 , intervals $-\bar{u}'u' \leq 0.045 : 0.01$, $0.045 \leq \bar{u}'u' \leq 0.12 : 0.015$, $0.12 \leq \bar{u}'u' \leq 0.2 : 0.02$, $0.2 \leq \bar{u}'u' \leq 0.4 : 0.05$; (b) $\bar{v}'v'$, minimum value contour 0.015 , intervals $\bar{v}'v' \leq 0.06 : 0.015$, $0.06 \leq \bar{v}'v' \leq 0.1 : 0.02$, $0.1 \leq \bar{v}'v' \leq 0.2 : 0.025$, $0.2 \leq \bar{v}'v' \leq 0.4 : 0.05$, $0.4 \leq \bar{v}'v' \leq 0.1 : 0.1$; (c) $-\bar{u}'v'$, -----, negative values; ———, positive values; absolute value of minimum contour 0.0075 , intervals $|\bar{u}'v'| \leq 0.0375 : 0.015$, $0.0375 \leq |\bar{u}'v'| \leq 0.1375 : 0.025$, $0.1375 \leq \bar{u}'v' \leq 0.2875 : 0.0375$.

3.6. The turbulent component

The phase variation of the (two-dimensional) turbulent kinetic energy, $\langle k \rangle \equiv (\langle u'^2 \rangle + \langle v'^2 \rangle)/2$, and the Reynolds shear stress, $\langle -u'v' \rangle$, is shown in figure 11. At $x = 2$, both signals are in phase for $y \geq 0.5$. Since $\langle -u'v' \rangle$ does not change sign in this region, which remains strongly influenced by the separated shear layer at all phases, small values of $\langle k \rangle$ are associated with small (absolute) values of $\langle -u'v' \rangle$ that result as free-stream fluid is drawn into the base region. Phases during which $\langle k \rangle$ and $\langle -u'v' \rangle$ reach a minimum occur with phases of high (negative) $\langle v \rangle$ (figure 9). Similarly, maxima in

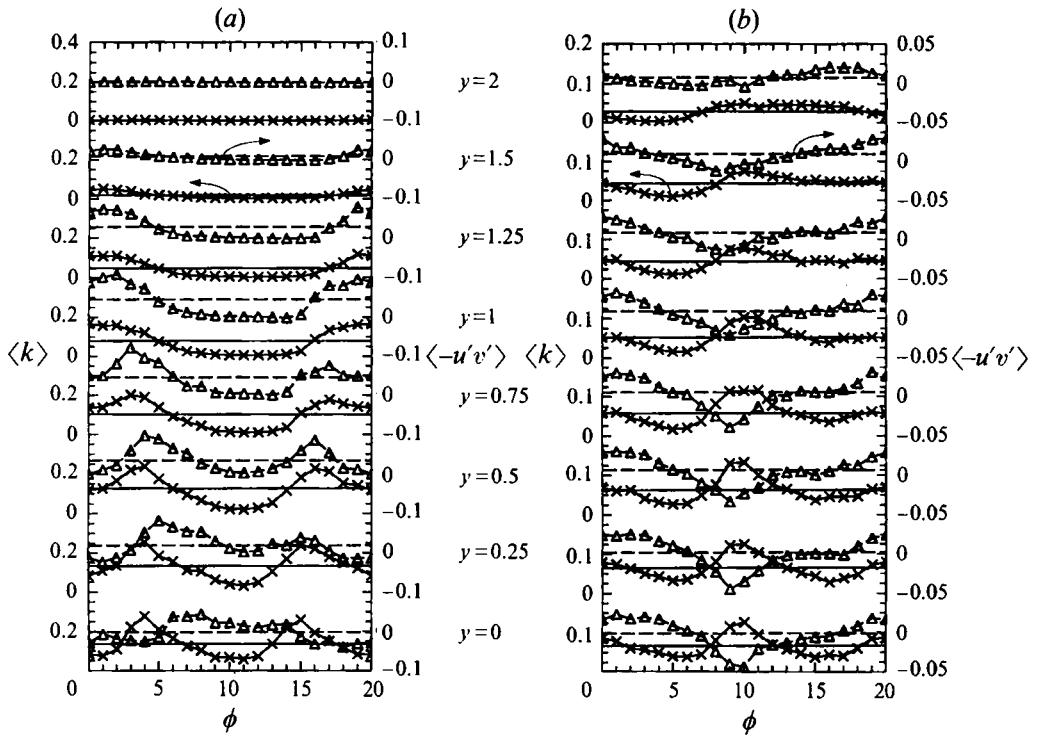


FIGURE 11. Variation with phase of $\langle k \rangle$, \times , and $\langle -u'v' \rangle$ Δ , at the same lateral locations at two sections, (a) $x = 2$ and (b) $x = 6$. Lines are drawn for visual clarity only; horizontal lines indicate average over all phases: —, $\langle k \rangle$; - - - -, $\langle -u'v' \rangle$.

$\langle k \rangle$ (and $\langle -u'v' \rangle$ for $y \geq 0.25$) occur with sharp transitions in $\langle v \rangle$. Only in the region near the centreline ($y < 0.25$) does the phase relationship between $\langle k \rangle$ and $\langle -u'v' \rangle$ (and also $\langle v \rangle$) become erratic. At $x = 6$, where $\langle -u'v' \rangle$ does change sign during a cycle, large (small) absolute values of $\langle -u'v' \rangle$ are associated with large (small) values of $\langle k \rangle$, so that even though local peaks in $\langle k \rangle$ and $\langle -u'v' \rangle$ differ in location in the near wake, this does not necessarily imply that the two quantities vary out of phase with each other at any given location.

The contours of the distribution of turbulent stresses (and also $\langle k \rangle$) in the wake are shown in figure 12. Peaks of $\langle u'^2 \rangle$ and $\langle v'^2 \rangle$ and hence of $\langle k \rangle$ coincide with vorticity peaks for $x > 2$. The large difference between the peak values of $\langle v'^2 \rangle$ and $\langle u'^2 \rangle$, particularly in the base region, is notable. The contours of $\langle k \rangle$ essentially follow those of $\langle v'^2 \rangle$, but are subtly influenced by $\langle u'^2 \rangle$; the mild streamwise asymmetry about the near-wake peak in $\langle v'^2 \rangle$ is accentuated in $\langle k \rangle$, such that a valley of low turbulence cuts across the wake just downstream of the peak $\langle k \rangle$ at $x = 5.8$ (see also HH). Previous studies have emphasized the correlation between streamline saddles with regions of high $\langle -u'v' \rangle$ (CC; Perry & Steiner 1987; Kiya & Matsumura 1987; HH). The present results (figure 12d) give limited support to this model since high $\langle -u'v' \rangle$ regions are indeed observed near saddle regions. Peaks in $\langle -u'v' \rangle$ tend however to be located consistently upstream of the streamline saddle and the vortex peak, and closer to the centreline. Double peaks in $\langle -u'v' \rangle$ are observed in the region $5 < x < 6$, and are also clearly seen in CC (phase (7,15)) and less so in HH at $x = 10$. They appear in the majority of phases throughout the measurement region, and are unlikely to be a

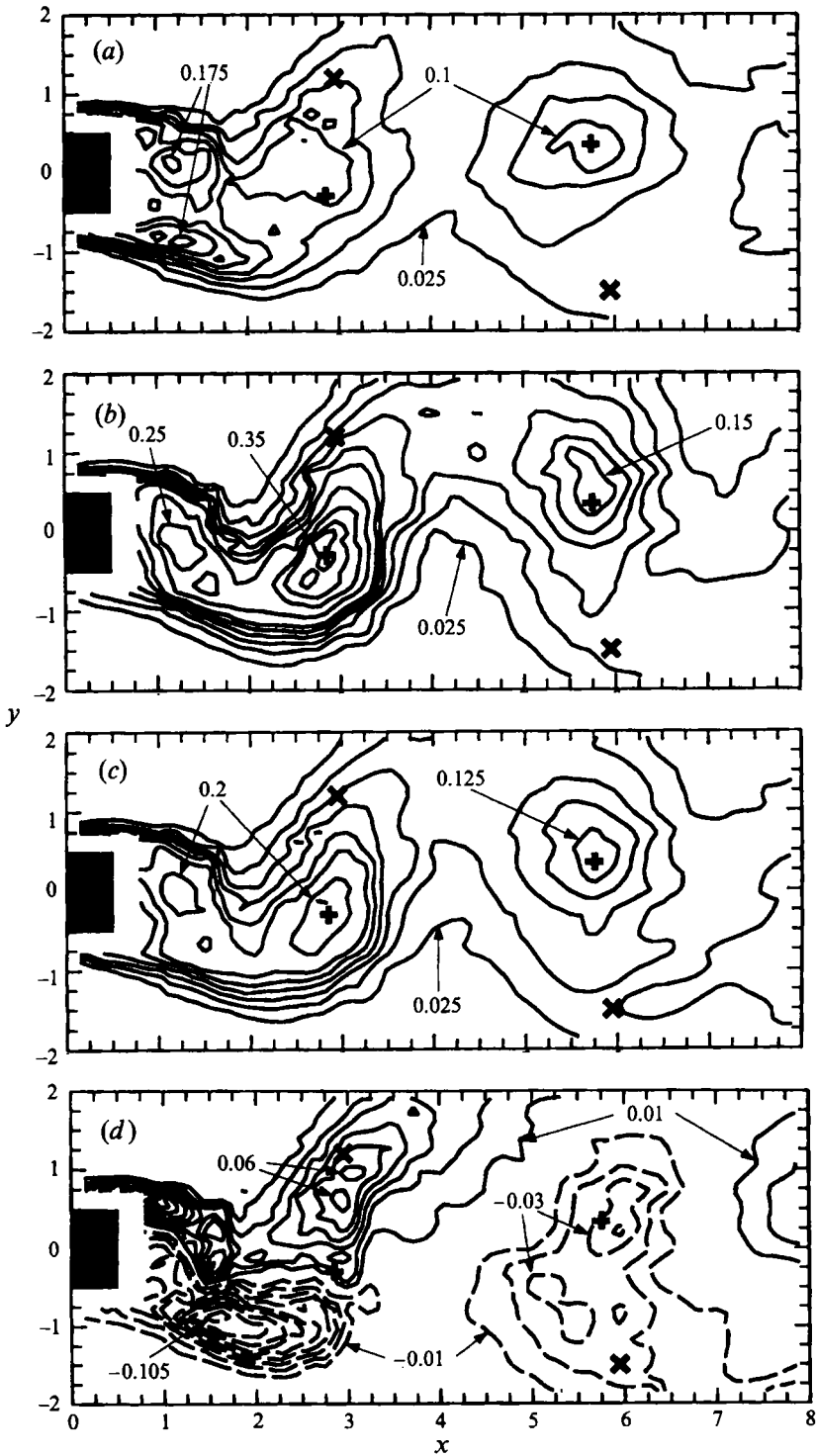


FIGURE 12. Contour plots of the turbulent stresses for phase (9,19): (a) $\langle u'^2 \rangle$, minimum contour 0.025, intervals $\langle u'^2 \rangle \leq 0.2 : 0.025$; (b) $\langle v'^2 \rangle$, minimum contour 0.025, intervals $\langle v'^2 \rangle \leq 0.15 : 0.025$, $0.15 \leq \langle v'^2 \rangle \leq 0.35 : 0.05$; (c) $\langle k \rangle$ (contour levels same as for $\langle v'^2 \rangle$); (d) $\langle -u'v' \rangle$: - - - -, negative values; —, positive values; absolute value of minimum contour: 0.01, intervals $0.01 \leq | \langle -u'v' \rangle | \leq 0.06 : 0.01$, $0.06 \leq | \langle -u'v' \rangle | \leq 0.12 : 0.015$.

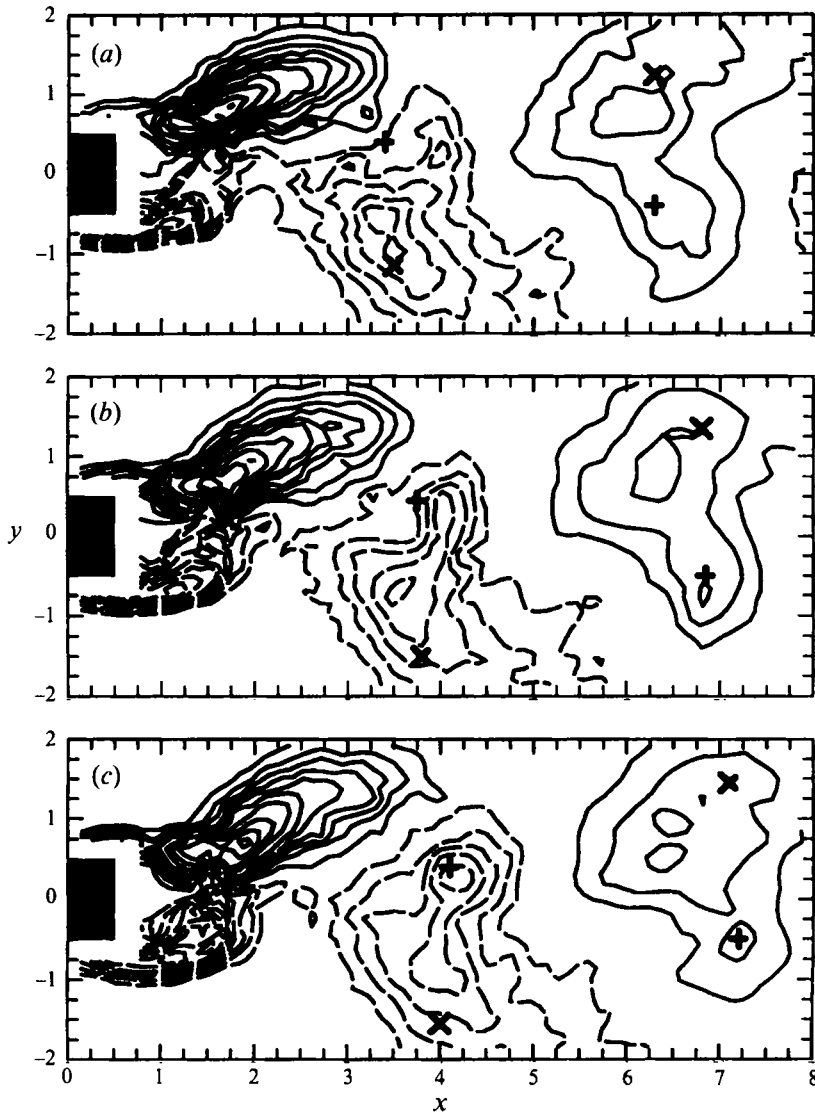


FIGURE 13. Contour plots of the Reynolds shear stress at three successive phases: (a) phase (1,11), (b) phase (2,12), (c) phase (3,13) showing the genesis of the local double peak in the $\langle -u'v' \rangle$ -distribution (contour intervals as in figure 12d)

statistical aberration, or to have resulted from phase jitter which would tend to smear rather than to produce a bimodal distribution.

The evolution of the double-peak feature is followed at successive phases in figure 13. At phase (9,19), the centre at $(x, y) \approx (2.9, -0.3)$ is located in a region of low $\langle -u'v' \rangle$ (figure 12d), consistent with recent models, and this remains so (though reflected about the centreline) at phase (1,11), when the vortex (at $(x, y) \approx (3.4, 0.5)$) is just being 'shed' and the corresponding peak $\langle -u'v' \rangle$ remains located away from the vorticity peak. A 'leg' then develops almost perpendicular to the main body of the $\langle -u'v' \rangle$ -contours, but parallel to the main body of the *upstream* $\langle -u'v' \rangle$ -contours. This is evident by phase (2,12) when values of $\langle -u'v' \rangle$ in the 'leg' become comparable to those nearer the saddle region, and by phase (3,13), the double-peak structure is

established. Similar features are seen farther downstream, although a weakening of the $\langle -u'v' \rangle$ -peaks near vortex peaks may be discerned. The results of HH closest to the cylinder (at $x = 10$) also clearly show a 'leg' of $\langle -u'v' \rangle$ extending through a vortex centre.

3.7. Turbulence production

In flow that is two-dimensional in the mean, the production, $\langle P \rangle$, of $\langle k \rangle$ is the sum of shear stress production, $\langle P \rangle_s$, and normal stress production, $\langle P \rangle_n$, where

$$\langle P \rangle_s = \langle -u'v' \rangle \langle \mathcal{S} \rangle = \langle -u'v' \rangle \left(\frac{\partial \langle u \rangle}{\partial y} + \frac{\partial \langle v \rangle}{\partial x} \right), \tag{3a}$$

$$\langle P \rangle_n = -\langle u'^2 \rangle \frac{\partial \langle u \rangle}{\partial x} - \langle v'^2 \rangle \frac{\partial \langle v \rangle}{\partial y}, \tag{3b}$$

$$= \left[\langle v'^2 \rangle - \langle u'^2 \rangle \right] \frac{\partial \langle u \rangle}{\partial x} \tag{3c}$$

and $\langle \mathcal{S} \rangle$ is (twice) the shear strain rate, and (3c) follows from continuity.

In the vortex-peak region, contours of $\langle \mathcal{S} \rangle$ (of a single sign) form a neck from one side of the cylinder to the other, with larger absolute values being attained on the saddle side (figure 14a). The contours of $\langle P \rangle_s$ (figure 14b) resemble those of $\langle -u'v' \rangle$ rather than $\langle \mathcal{S} \rangle$. Peaks in $\langle P \rangle_s$ and $\langle -u'v' \rangle$ generally coincide, but are distinctly located away from local peaks in $\langle \mathcal{S} \rangle$, at least in the near wake. The peak and the 'leg' seen in the $\langle -u'v' \rangle$ -distribution are weakly present in the $\langle P \rangle_s$ -distribution. A similar feature was noted by HH and attributed to large strain rates in that region and to spanwise undulations of the vortex structure. Contours of $\langle P \rangle_n$ (computed using (3b)) are erratic (figure 14c), and areas of negative $\langle P \rangle_n$ are more prominent. To some extent, this is attributed to $\langle P \rangle_n$ often being a difference of two 'large' numbers and to its sensitivity to continuity not being satisfied by the measured velocity field. Peak magnitudes of $\langle P \rangle_n$ and $\langle P \rangle_s$ are comparable in both the base and the near-wake regions, whereas, in circular-cylinder measurements farther downstream (HH), the former was reported to be generally three times larger than the latter. In the vicinity of vortex peaks, $\langle P \rangle_s$ is small though not always negligible, but $\langle P \rangle_n$ may be substantial, especially in the base region where large differences between $\langle u'^2 \rangle$ and $\langle v'^2 \rangle$ and the elongated shape of the vortex structures give rise to large normal strains. Unlike $\langle P \rangle_s$, $\langle P \rangle_n$ is significant in the region between successive structures. Regions of negative $\langle P \rangle_n$ are also consistently observed in vortex-peak regions (see also HH). This arises where $\partial \langle u \rangle / \partial x < 0$ (or $\partial \langle v \rangle / \partial y > 0$), since $\langle v'^2 \rangle > \langle u'^2 \rangle$ in most regions of the flow. Whereas streamwise gradients are negligible in the mean near-wake flow, they are significant in the phase-averaged flow, particularly when coupled with $(\langle v'^2 \rangle - \langle u'^2 \rangle) > |\langle -u'v' \rangle|$.

The patchy features seen in the $\langle P \rangle_n$ -contours appear also in the $\langle P \rangle$ -contours (figure 14d). A region of high $\langle P \rangle$ extends through the vortex peak region at $(x, y) \approx (2.75, -0.25)$ to $(x, y) \approx (3.2, 0.6)$, which is near a streamline saddle. Since $\langle P \rangle_s$ is negligible in the vortex peak region, the local peak in $\langle P \rangle$ there is due to high values of $\langle P \rangle_n$. Farther downstream, $\langle P \rangle_n$ still contributes to $\langle P \rangle$ in vortex-peak regions, but $\langle P \rangle_s$ is no longer negligible. Remnants of negative $\langle P \rangle_n$ are seen in $\langle P \rangle$ in the near wake, e.g. at $x = 5.5$. Previous discussions of negative turbulence production (e.g. Hussain 1983, 1986) have been concerned primarily with negative *mean* production in shear layers, which was explained in terms of contributions due to 'coherent' Reynolds stresses such as $-\overline{u\tilde{v}}$. From (3), negative $\langle P \rangle$ may occur where

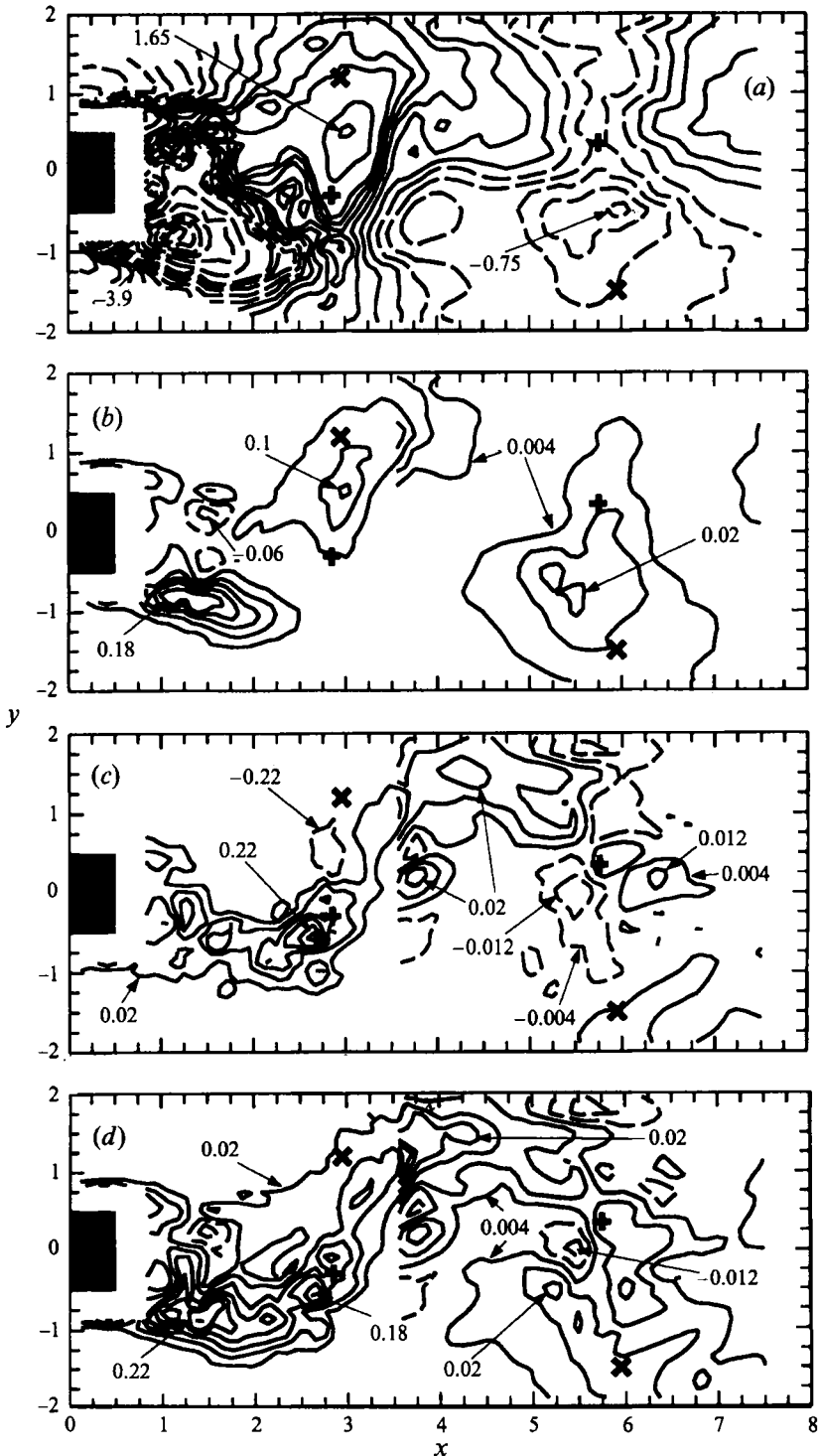


FIGURE 14. Contour plots for phase (9,19) of (a) $\langle \mathcal{P} \rangle$, contour intervals $|\langle \mathcal{P} \rangle| \leq 0.75 : 0.15$, $|\langle \mathcal{P} \rangle| \geq 0.75 : 0.45$; (b) $\langle P \rangle_s$, contour intervals for $x \leq 3.5$ are 0.04, for $x > 3.5$ are 0.008; (c) $\langle P \rangle_n$, contour intervals same as for $\langle P \rangle_s$, (d) $\langle P \rangle$, contour intervals same as for $\langle P \rangle_s$. - - - - -, negative values; ———, positive values.

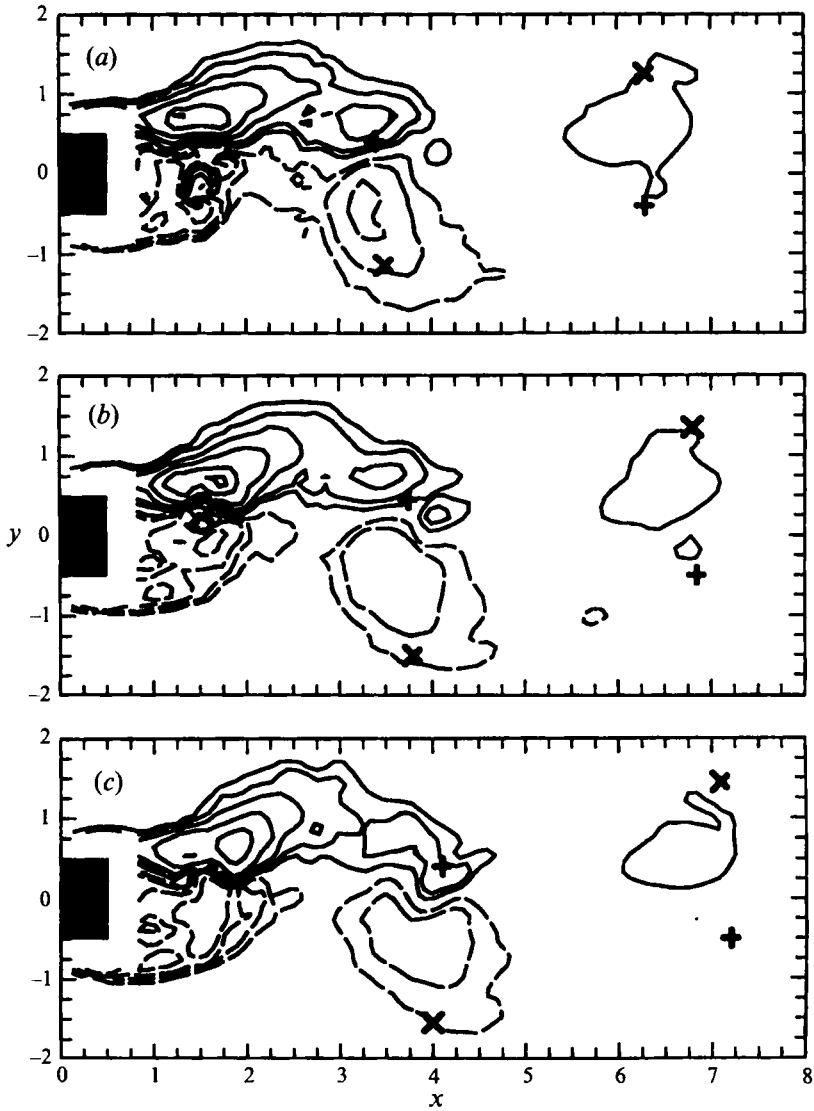


FIGURE 15. Contour plots of the production term, $\langle P \rangle_{(-u'v')}$, in the transport equation for $\langle -u'v' \rangle$ at three successive phases: (a) phase (1,11), (b) phase (2,12), (c) phase (3,13), contour intervals: ± 0.025 , ± 0.05 , ± 0.1 , ± 0.2 , ± 0.4 , ± 0.6 .

$|\langle P \rangle_s| \ll |\langle P \rangle_n|$ and $\langle P \rangle_n < 0$, such as in the vicinity of a vortex peak. The results of CC did not show any region of negative $\langle P \rangle$, but their contours do indicate a necking or saddle point in $\langle P \rangle$ near a vortex peak. Because of the well-known importance of transport effects on $\langle k \rangle$, the contours of $\langle P \rangle$ do not provide any direct insight concerning the $\langle k \rangle$ -distribution.

The anomalous double peaks in the $\langle -u'v' \rangle$ -distribution prompted an examination of the contours of the production term in the equation for $\langle -u'v' \rangle$, namely

$$\langle P \rangle_{(-u'v')} = \langle u'^2 \rangle \frac{\partial \langle v \rangle}{\partial x} + \langle v'^2 \rangle \frac{\partial \langle u \rangle}{\partial y}. \tag{4}$$

These are plotted in figure 15 for phases 1–3. With a striking exception, the $\langle P \rangle_{(-u'v')}$

contours are similar to the $\langle -u'v' \rangle$ -contours, positive $\langle P \rangle_{\langle -u'v' \rangle}$ being associated with positive $\langle -u'v' \rangle$. Peak values of $\langle P \rangle_{\langle -u'v' \rangle}$ are found notably away from the streamline saddle. The striking exception occurs in precisely the anomalous vortex peak region, where high values of $\langle -u'v' \rangle$ were previously observed. In this region, e.g. $(x, y) \approx (4, 0.5)$, the signs of $\langle P \rangle_{\langle -u'v' \rangle}$ and $\langle -u'v' \rangle$ surprisingly differ. The anomalous peak in $\langle -u'v' \rangle$ near vortex centres cannot therefore be attributed to locally (relatively) high values of $\langle P \rangle_{\langle -u'v' \rangle}$ (of the same sign), but points rather to the importance of non-local transport effects, which was hinted at by the same-signed $-\tilde{u}\tilde{v}$ -contours extending from one side of the centreline to the other of figure 10(c).

4. Further discussion

4.1. Streamwise variation of integral characteristics

The streamwise separation of successive vorticity peaks in the near-wake region, $l_x \approx 5.8$, is larger than that found for the circular case, $l_x \approx 4.3$ (CC) or the bluff plate, $l_x \approx 5.25$ (Fage & Johansen 1927), but approximately the same as that for a rectangular case, $l_x \approx 5.9$ (Bearman & Trueman 1972). Since l_x is the distance travelled by a vortex in one cycle, the ratio of l_x for the square and the circular cases, $5.8/4.3 \approx 1.35$, should be approximately equal to the ratio of the reciprocal of the Strouhal numbers (namely $0.179/0.132 \approx 1.36$, assuming that the vortex celerities do not differ greatly). A similar result is obtained if l_x and St of the bluff plate or the rectangle are considered. The shape of the vortex contours in the near wake is similar for both geometries, and so the increase in the streamwise lengthscale in the square geometry implies an increase in the cross-stream lengthscale, consistent with the observed larger wake width. Larger streamwise lengthscales also imply smaller mean streamwise gradients, consistent with the slower recovery of the centreline \bar{u}^f . The ratio, $y_c/(l_x/2)$, for the square cylinder is larger than that of the circular cylinder (0.19 compared to 0.16), but smaller than the bluff plate (0.25, Fage & Johansen, 1928). All are however smaller than the value, 0.28, predicted by the classical von Kármán analysis (1912).

Peak vorticities, $\langle \omega \rangle_p$, decay rapidly in the base region and more slowly in the near wake (figure 16a). In the base region, the two separated shear layers with oppositely signed vorticity interact more directly and vigorously, resulting in substantial cancellation of vorticity. In the near wake, after a vortex structure has been shed, interaction with other structures with vorticity of the opposite sign is more 'passive'; reduction of $\langle \omega \rangle_p$ is due to a slower more 'diffusive'-like process linked more to entrainment of free-stream fluid.

The circulation, Γ , associated with the shed vortex, was estimated from a surface quadrature of $|\langle \omega \rangle|$, i.e.

$$\Gamma(x_c) = \sum_{i,j} \langle \omega \rangle_{i,j} \Delta A_{i,j}, \quad (5)$$

in a manner similar to the determination of the vorticity centroid location (see §3.4). Values of Γ were $\approx 60\%$ higher than those reported for the circular-cylinder case. The difference is due not only to higher values of $\langle \omega \rangle_p$ ($\approx 25\%$ higher in the near-wake region), but also to larger lengthscales. The streamwise variation of Γ , normalized by the initial circulation, Γ_0 , discharged into the wake during a cycle, is plotted in figure 16(b). Γ_0 was estimated from the base pressure coefficient, C_{pb} , according to

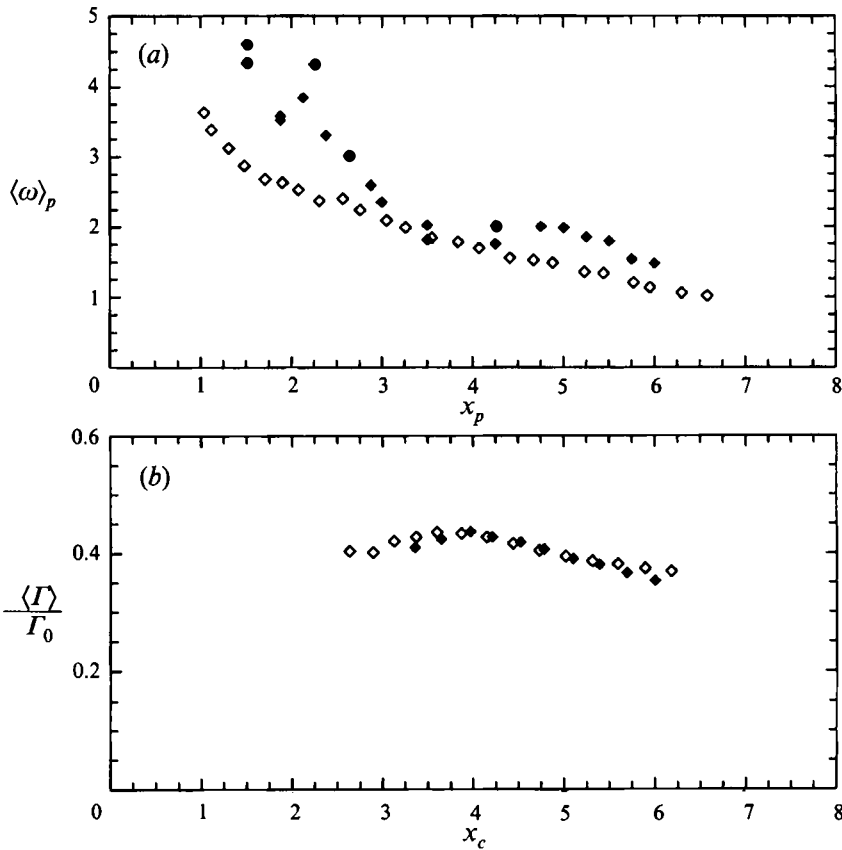


FIGURE 16. Downstream decay of (a) peak vorticity, $\langle \omega \rangle_p$, (b) Γ / Γ_0 ($\Gamma_0 = 10$); \blacklozenge , present results; \diamond , CC ($\Gamma_0 = 5.9$).

the approximate bluff-body relation (Roshko 1954; Bearman & Obasaju 1982),

$$\Gamma_0 = \frac{1 - C_{pb}}{2 St}. \tag{6}$$

C_{pb} was not measured, but over the same Re range Bearman & Obasaju (1982) reported a $C_{pb} \approx -1.6$ for stationary square cylinders, implying $\Gamma_0 \approx 10$ for the present case compared to $\Gamma_0 \approx 5.9$ for the circular cylinder (CC). The streamwise variation of Γ / Γ_0 is very similar, both qualitatively and quantitatively, to that observed by CC. In the near wake, Γ / Γ_0 slowly decays with an average rate of decay of $\approx 10\%$ per diameter of travel (cf. 8% decay rate in CC). figure 16(a) indicates an at least 60% decrease in $\langle \omega \rangle_p$, indicating that the reduction in Γ in the base region is due primarily to reduced values of $\langle \omega \rangle$.

Peak values of the ‘periodic’ stresses decay sharply in the base region (figure 17), but then flatten out in the near wake, reminiscent of the decay of $\langle \omega \rangle_p$. $(\bar{v}\bar{v})_{max}$ attains a maximum at $x \approx 1.75$, approximately the position at which a vortex structure is ‘shed’, or as discussed below, the downstream limit of the vortex formation region. Beyond the maximum, $(\bar{v}\bar{v})_{max}$ is substantially larger than $(\bar{u}\bar{u})_{max}$, typically by a factor of 4–6. Because of differences in streamwise lengthscales in the near wake, any direct quantitative comparison of the values for a square and a circular-cylinder should be cautiously interpreted. The sharp decay of the periodic stresses seen in the present

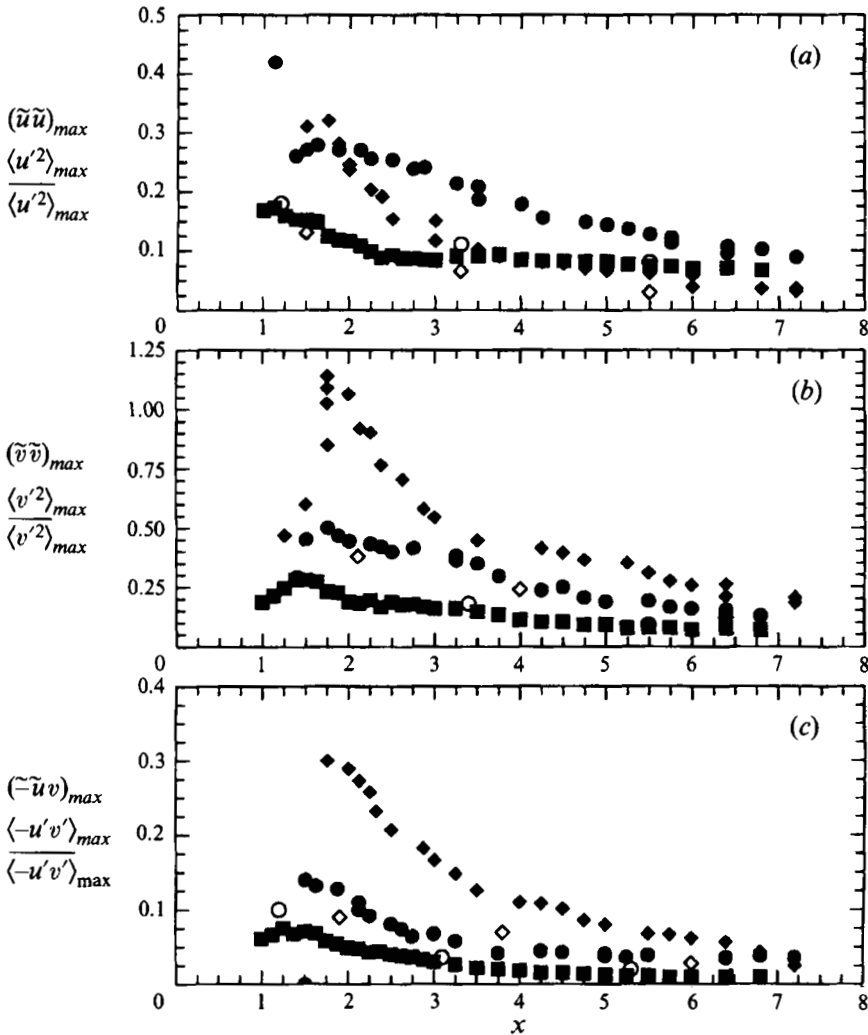


FIGURE 17. Comparison of streamwise variation of peak values of various characteristics: (a) \blacklozenge , $(\tilde{u}\tilde{u})_{max}$; \bullet , $\langle u'^2 \rangle_{max}$; \blacksquare , $\overline{\langle u'^2 \rangle}_{max}$; (b) \blacklozenge , $(\tilde{v}\tilde{v})_{max}$; \bullet , $\langle v'^2 \rangle_{max}$; \blacksquare , $\overline{\langle v'^2 \rangle}_{max}$; (c) \blacklozenge , $(-\tilde{u}\tilde{v})_{max}$; \bullet , $\langle -u'v' \rangle_{max}$; \blacksquare , $\overline{\langle -u'v' \rangle}_{max}$; closed symbols: present results; open symbols – CC.

results is hardly noticeable in the circular cylinder results. The present levels are more than $\approx 200\%$ larger than those of the circular cylinder in the base region, and more than $\approx 70\%$ in the near wake.

Compared to the decay in the peak values of the periodic component and the vorticity, the decay of the peaks in the turbulent component are surprisingly gradual. In the case of $\langle u'^2 \rangle_{max}$, this leads to $\langle u'^2 \rangle_{max}$ being larger than $(\tilde{u}\tilde{u})_{max}$ throughout much of the measurement region. While $(\tilde{v}\tilde{v})_{max} > \langle v'^2 \rangle_{max}$ throughout, the difference narrows towards the end of the measurement region, and farther downstream, $\langle v'^2 \rangle_{max}$ may become dominant. The small disparity between the maximum normal turbulent stresses contrasts with the already noted much larger disparity between the maximum normal periodic stresses. A narrowing with downstream distance of the difference between the maximum and the average (over all phases) turbulent stresses is also noted, at least for the normal stresses. In the base region, stronger incursions of

free-stream fluid across the centreline would bring longer periods of low turbulence, which together with larger maximum values, would imply larger deviations from the average value.

4.2. A scaling argument

A scaling argument, based on the observation that Γ/Γ_0 is approximately the same for both the square and the circular geometries, sheds light on the relative magnitudes of the periodic and turbulent quantities as well as on mean integral characteristics. Γ is a product of a velocity scale, \mathcal{U} , and a lengthscale, \mathcal{L} :

$$\frac{\Gamma_{sq}}{\Gamma_{circ}} = \frac{(\Gamma_0)_{sq}}{(\Gamma_0)_{circ}} \approx \frac{10}{5.9} \tag{7a}$$

$$\sim \frac{(\mathcal{U}\mathcal{L})_{sq}}{(\mathcal{U}\mathcal{L})_{circ}}, \tag{7b}$$

where the subscripts *sq* and *circ* indicate the square and the circular case. In the near wake, $\mathcal{L}_{sq}/\mathcal{L}_{circ} \approx 1.35$, where $\mathcal{L} \sim l_x$. Hence, $\mathcal{U}_{sq}^2/\mathcal{U}_{circ}^2 \approx 1.6$, roughly agreeing with the observed ratio of magnitudes of peak periodic ‘stresses’ in the near wake.

This scaling is consistent with observed differences in the drag coefficient, C_D , for the two geometries. With the thin shear-layer approximation, the drag force is proportional to the momentum integral, $F_D \propto \int_{-\infty}^{\infty} \bar{u}'(\bar{u}'_{\infty} - \bar{u}') dy$ (Tennekes & Lumley 1972). Beyond the base region, the following scaling relations apply: $\bar{u}' \sim \bar{u}'_{\infty}$, and $(\bar{u}'_{\infty} - \bar{u}') \sim \mathcal{U}$, so that $F_D \sim \bar{u}'_{\infty} \mathcal{U} \mathcal{L}$, or $F_D \sim \mathcal{U} \mathcal{L}$, since $\bar{u}'_{\infty} = 1$. The ratio of drag coefficients should therefore be

$$\frac{(C_D)_{sq}}{(C_D)_{circ}} \approx \frac{\mathcal{U}_{sq}}{\mathcal{U}_{circ}} \frac{\mathcal{L}_{sq}}{\mathcal{L}_{circ}} \approx \sqrt{1.6} \times 1.35 = 1.7, \tag{8}$$

which is consistent with the value of $2.1/1.25 = 1.68$ observed. Equation (8) is more directly expressed as $(C_D)_{sq}/(C_D)_{circ} \sim (\Gamma_0)_{sq}/(\Gamma_0)_{circ} = 1.7$, or alternatively, $C_D/\Gamma_0 \approx$ constant. Table 2 shows values of C_D/Γ_0 for various symmetric bluff-body flows with drag coefficients varying over an order of magnitude, including cases of critical flow around a circular cylinder and the peak drag case of a rectangular bluff body (width-to-thickness ratio, $B/A = 1.62$). For the rectangular (including the peak drag case), square and circular cross-sections for ‘subcritical’ flows, $C_D/\Gamma_0 \approx 0.22$; even for critical flow around a circular cylinder and flow around a bluff plate, the values are not greatly different. A relation, $C_D/\Gamma_0 = 0.28$ had already been proposed by Fage & Johansen (1927; see also Roshko 1955, and Bearman 1967) based on the von Kármán vortex street drag formula, where the value of 0.28 is obtained from the theoretical ‘stable’ value of $y_c/(l_x/2)$, which as was seen above is significantly larger than the observed value.

The ratio of lengthscales in the \mathcal{L} region for the two geometries is less clear. If it is hypothesized that $\mathcal{L}_{sq} \sim \mathcal{L}_{circ} \sim \mathcal{L}$, then $\mathcal{U}_{sq}^2/\mathcal{U}_{circ}^2 \sim [(\Gamma_0)_{sq}/(\Gamma_0)_{circ}]^2 \approx 2.9$, roughly agreeing with observed ratios. A candidate for this common lengthscale is the length of the vortex formation region proposed by Gerrard (1966). CC defined this as the point at which mean vorticity first becomes negligible upstream of the saddle of the shed vortex. In the present results, this occurs between $x = 1.5$ and $x = 1.75$, which is similar to the $x = 1.6$ reported by CC for the circular cylinder. This hypothesis is not necessarily strongly dependent on the choice of origin at the centre of the cylinder. An alternative origin might be the downstream edge of the cylinder, in which case the length of the vortex formation region is the distance from the farthest downstream solid boundary. This choice of an origin would still be consistent with

Geometry	Source	$Re (\times 10^{-4})$	B/A	St	$-C_{pb}$	C_D	Γ_0^i	C_D/Γ_0
Rectangular 	1	3	3.8	0.131	1.41	2.16	9.3	0.23
	1	1.9	1.62	0.128	2.35	2.80	12.9	0.22
	1	1.3	1	0.132	1.43	2.16	12.9	0.22
	2	2.1	1	0.13	1.6 ²	2.1 ³	10	0.21
Circular 	3	14.0	n/a	0.179	1.21	1.24	5.9	0.21
	4	n/a	n/a	0.187	1.02	1.2 ⁴	4.8	0.22
	5	40	n/a	0.46	0.24	0.23	1.3	0.17
Bluff plate 	6	n/a	n/a	0.146	1.38	2.13	8.15	0.26

n/a = not available or not applicable

Sources: 1) Norberg (1993), 2) present results, 3) CC, 4) Fage & Johansen (1928), 5) Bearman (1969), 6) Fage & Johansen (1927).

¹ computed using equation (6), except in the case of CC, which was taken directly from their paper (based on the measured velocity at separation).

² value taken from Bearman & Obasaju (1982).

³ estimated from momentum integral using mean velocity profiles.

⁴ a value for C_D was not given, so a literature value of 1.2 was assumed.

TABLE 2. Values of C_D/Γ_0 for symmetric bluff bodies

the hypothesis that the base-region lengthscales for the two cases are comparable. The comparison should be qualified, since the size of the formation region is known to vary with the free-stream turbulence level, which differs in the two cases.

Since, in the near wake, the ratio of peak magnitudes for the square cylinder to those for the circular cylinder is approximately the same as for the periodic stresses, the scaling argument for periodic stresses could be applied to the turbulent stress and would give reasonable estimates. In the base region, however, the peak values of the turbulent stresses are typically only about 50% larger than those reported for a circular-cylinder, dramatically different from the more than 200% disparity in the case of peak periodic stresses. The scaling argument requires modification in applying it to the base region. For the turbulent characteristics in the base region, it is argued that the appropriate lengthscale is not the length of the vortex formation region, but rather the cross-stream wake width. This is identical to the traditional model of the steady far wake, but is arguably also true of the unsteady base region. The cross-stream scale for the square cylinder is evidently larger than that for the circular cylinder; the (global) mean width of the square-cylinder wake is $\approx 25\%$ wider than that of the circular cylinder wake in the base region. With a ratio of lengthscales based on mean wake widths, the peak turbulent stresses for the square cylinder would, according to the scaling argument, be $\approx 60\%$ larger than those for the circular cylinder, in rough agreement with the observed values. Thus, in the base region, whereas streamwise lengthscales are important for periodic motion, cross-stream lengthscales dominate where the turbulent motions are concerned.

4.3. *The base region*

The evolution of vortex structures in the base region contrasts with their quasi-equilibrium state in the near wake. A sequence of $\langle\omega\rangle$ -contours in the base region at different phases is shown in figure 18. Overlaid on these are contours showing regions of high $\langle k \rangle$ (figures 18*a, d, g, j, m*), high $\langle -u'v' \rangle$ (figure 18*b, e, h, k, n*), and high $\langle P \rangle$ (figures 18*c, f, i, l, o*). In phase (1,11), a vortex has just been shed from the top, signalled by the 'necking' of the (negative) vorticity contours (the length of the vortex formation region was estimated from such a necking region). In addition to the high- $\langle P \rangle$ region expected near the saddle region, another is observed at $(x, y) \approx (3.3, 0.3)$ surprisingly near a vorticity peak. By phase (5,15), the development of a clear vorticity peak (at $(x, y) \approx (2.1, 0)$) is accompanied by downward indentations in the (+)-vorticity contours near the cylinder, resulting in a vorticity saddle at $(x, y) \approx (1.5, -0.8)$. Going from phase (1,11) to phase (5,15), the vorticity peak has increased in magnitude, indicating a tendency to vorticity concentration. The high- $\langle -u'v' \rangle$ contours contained within high- $\langle\omega\rangle$ contours of a single sign (e.g. at $(x, y) \approx 1.2, -0.75$) in phase (1,11) differ from those on the opposite side of the cylinder as well as those farther downstream, in being located in high- $\langle\omega\rangle$ regions, precisely as in traditional models of shear-layers.

At the same time that, on the upper side, a vortex structure is shed, on the lower side, the separated shear layer decelerates, a vorticity saddle is formed, and the location of the peak $\langle -u'v' \rangle$ moves downstream. By phase (7,17), the vorticity saddle and the $\langle -u'v' \rangle$ -peak coincide. $\langle -u'v' \rangle$ is not necessarily negligible in the separated shear layer, for a saddle point in the $\langle -u'v' \rangle$ -distribution may be formed between the shear layer region and the vorticity saddle. As the vortex structure is about to be shed (phase (9,19) or phase (1,11)), the $\langle -u'v' \rangle$ -peak moves from the vorticity saddle towards the zero- $\langle\omega\rangle$ region. At shedding, the $\langle -u'v' \rangle$ -peak is found in regions of

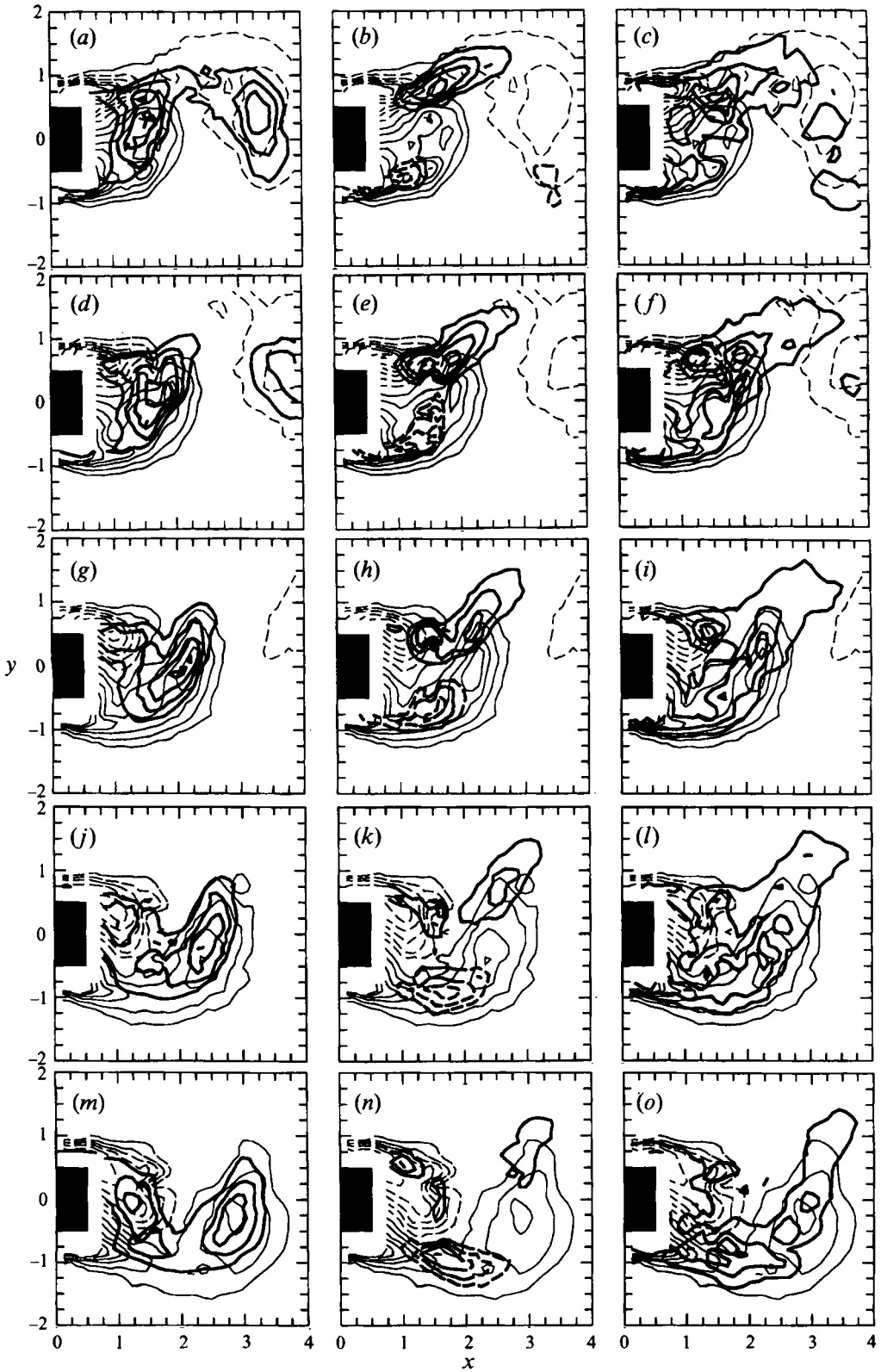


FIGURE 18. For caption see facing page.

negligible $\langle \omega \rangle$, but the region is no longer a vorticity saddle (though it may be a streamline saddle, see the Appendix).

Peaks in $\langle k \rangle$ are not always associated with a single structure as is the case in the near wake. In phases (1,11) and (9,19), a double peak is observed. A small peak is found between two structures at a zero- $\langle \omega \rangle$ location near the $\langle -u'v' \rangle$ -peak. The more extensive peak is entirely within one structure, situated away from the high $\langle -u'v' \rangle$ -region, but only at a later phase do the $\langle k \rangle$ -peak and $\langle \omega \rangle$ -peak overlap. The high- $\langle k \rangle$ region first straddles the zero- $\langle \omega \rangle$ line, and then the $\langle k \rangle$ -peak that originated in the peak- $\langle \omega \rangle$ shear-layer region grows in extent, and moves downstream, such that the $\langle -u'v' \rangle$ - and the $\langle k \rangle$ -peaks become separated. The little decay in the peak magnitude of $\langle k \rangle$ between the attached and the shed structure differs from the much faster decay in $\langle -u'v' \rangle$ and $\langle \omega \rangle$.

Both $\langle k \rangle$ and $\langle -u'v' \rangle$ may influence the form of the $\langle P \rangle$ -contours. Here $\langle k \rangle$ may also be used as a proxy for $(\langle v'^2 \rangle - \langle u'^2 \rangle)$, since $\langle v'^2 \rangle$ is the dominant component. The $\langle P \rangle$ -peak is found close to the $\langle -u'v' \rangle$ -peak, but $\langle P \rangle$ may still be substantial where $\langle -u'v' \rangle$ is zero because $\langle k \rangle$ is large. Even where $\langle -u'v' \rangle$ dominates, large values of $\langle k \rangle$ may displace the $\langle P \rangle$ -peak away from the $\langle -u'v' \rangle$ -peak. In the early phases, before the (+)-vorticity saddle is formed, $\langle P \rangle$ is high in the separated shear-layer region, but with the formation of the vorticity saddle, a high- $\langle P \rangle$ region appears (phase (7,17)), much like the $\langle -u'v' \rangle$ -peak. Later, again like the $\langle -u'v' \rangle$ -peak, the $\langle P \rangle$ -peak moves away from the vorticity saddle, first towards a region of zero $\langle \omega \rangle$ between the vortex structures, and then forms double peaks, one in each structure.

4.4. Asymmetries, anomalies, and conceptual models

Conceptual models of the near wake portray the high- $\langle P \rangle$ region as symmetric about the saddle and aligned with the diverging separatrix. In this study, regions of peak $\langle -u'v' \rangle$ and $\langle P \rangle$, though aligned with the diverging separatrix, were located upstream of the saddle and closer to the centreline. The data of CC are believed to support this observation, though the smaller lengthscales blur the distinction between the $\langle -u'v' \rangle$ -peak and $\langle P \rangle$ -peak on the one hand and a streamline saddle on the other. A cross-stream asymmetry is inherent at the saddle. The diverging separatrix directed towards the free stream enters a region of lower turbulence levels and smaller strain rates. Hence, less turbulence is produced along it than along its counterpart, the diverging separatrix directed towards the centreline, which enters a region of higher turbulence levels and larger strain rates. CC argued that high $\langle P \rangle$ occurs in the saddle region because of high strain rates there rather than because of high stresses. Though it may be misleading to consider *only* shear strain, the $\langle \mathcal{S} \rangle$ -peak does not coincide with either the $\langle P \rangle_s$ -peak or the $\langle P \rangle$ -peak or with the streamline saddle. Anomalous features of the $\langle -u'v' \rangle$ -distribution, e.g. double peaks and peaks located near vortex centres, point to the importance of transport effects not only on $\langle k \rangle$ as is generally accepted but also on $\langle -u'v' \rangle$ at least in the base region. The possible importance of negative $\langle P \rangle$ in determining features of the $\langle -u'v' \rangle$ -distribution has also been little explored.

In the base region, the region of peak $\langle -u'v' \rangle$ and $\langle P \rangle$ may, at different phases, be

FIGURE 18. Contour plots of $\langle k \rangle$ (a, d, g, j, m), $\langle -u'v' \rangle$ (b, e, h, k, n), and $\langle P \rangle$ ((c, f, i, l, o) superimposed on contour plots of $\langle \omega \rangle$ in the base region; phase (1,11) (a-c), phase (3,13) (d-f), phase (5,15) (g-i), phase (7,17) (j-l), and phase (9,19) (m-o). Thick lines represent $\langle k \rangle$, $\langle -u'v' \rangle$, and $\langle P \rangle$, thin lines represent $\langle \omega \rangle$; solid and dashed lines represent positive and negative values respectively.

associated more with a vorticity saddle, or with a region of zero $\langle \omega \rangle$, or be entirely within a vortex structure but away from any vorticity saddle (though possibly at a streamline saddle). In the development of the vorticity saddle at $(x, y) \approx (1.7, -0.8)$ during phase (3,13) to phase (7,17), the vorticity saddle, in spite of relatively high values of $\langle \omega \rangle$, seems to be the key feature since the peak $\langle -u'v' \rangle$ occurs there. It is argued in the Appendix that, in phases (3,13) to (5,15), the vorticity saddle cannot be a streamline saddle. The influence of the shear layer and vortex structure on the other side seems relatively unimportant during these phases. Immediately prior to shedding (phases (9,19) in the bottom half and (1,11) in the upper half of the flow region), the nose of the negatively signed vortex structure seems to interact more vigorously with the positively signed vorticity saddle in terms of mixing of fluid elements of opposite vorticities. Hence, the peak $\langle -u'v' \rangle$ moves from the vorticity saddle to a region between the opposite-signed structures, i.e. a region of zero $\langle \omega \rangle$ but high vorticity gradients. A vorticity saddle is a prerequisite for this stage, but the vorticity saddle itself ceases to be dominant with regard to turbulence production.

5. Summary

The unsteady turbulent flow around a square cylinder was studied experimentally by obtaining phase-averaged velocity statistics from two-component laser-Doppler velocimetry measurements. The qualitative features observed agreed in some respects with previous measurements of flow around a circular cylinder and other bluff bodies. The distinction between the base region and the near wake emphasized differences in the flow characteristics and their evolution. Quantitative comparisons with the circular cylinder showed that lengthscales were larger not only in the cross-stream but, in the near wake, also in the streamwise direction. Peak values of both turbulent as well as 'periodic' stresses were also significantly larger than those measured behind the circular cylinder. A scaling argument based on the circulation discharged into the wake was proposed to account for the differences in velocity scales for both periodic and turbulent components. The decay of the 'periodic' stresses was found to be noticeably faster than that of the turbulent stresses in the base region. It was suggested that, in the base region, the periodic component was governed by the streamwise size of the vortex formation region, while the turbulent component was governed by the wake width.

Two related features of the near wake were highlighted. A double peak in the $\langle -u'v' \rangle$ -distribution associated with a vortex structure is found in the near wake, with one peak occurring in the vortex peak region. The second feature concerns the possible importance of turbulence production in regions close to the vortex centre due to large values of normal Reynolds stresses. This could possibly explain the centre peak in $\langle -u'v' \rangle$, although non-local transport effects also are likely to play a role. As the vortex peak moves downstream and becomes more circularly symmetric, the contribution due to the normal (in conventional coordinates) production and, hence, the centre peak in $\langle -u'v' \rangle$ decreases in relative importance. Flow topology was examined and a distinction between vorticity and streamline saddles was drawn. In the base region, a vorticity saddle is not necessarily a point of negligible spanwise vorticity, and peaks in $\langle -u'v' \rangle$ may, at different stages of the shedding process, be associated with the separated shear layer, the vorticity saddle, the region of zero vorticity or the streamline saddle. While peak production was often associated, if not necessarily identical, with peak Reynolds shear stresses, large values of turbulence production were also observed near vortex peaks.

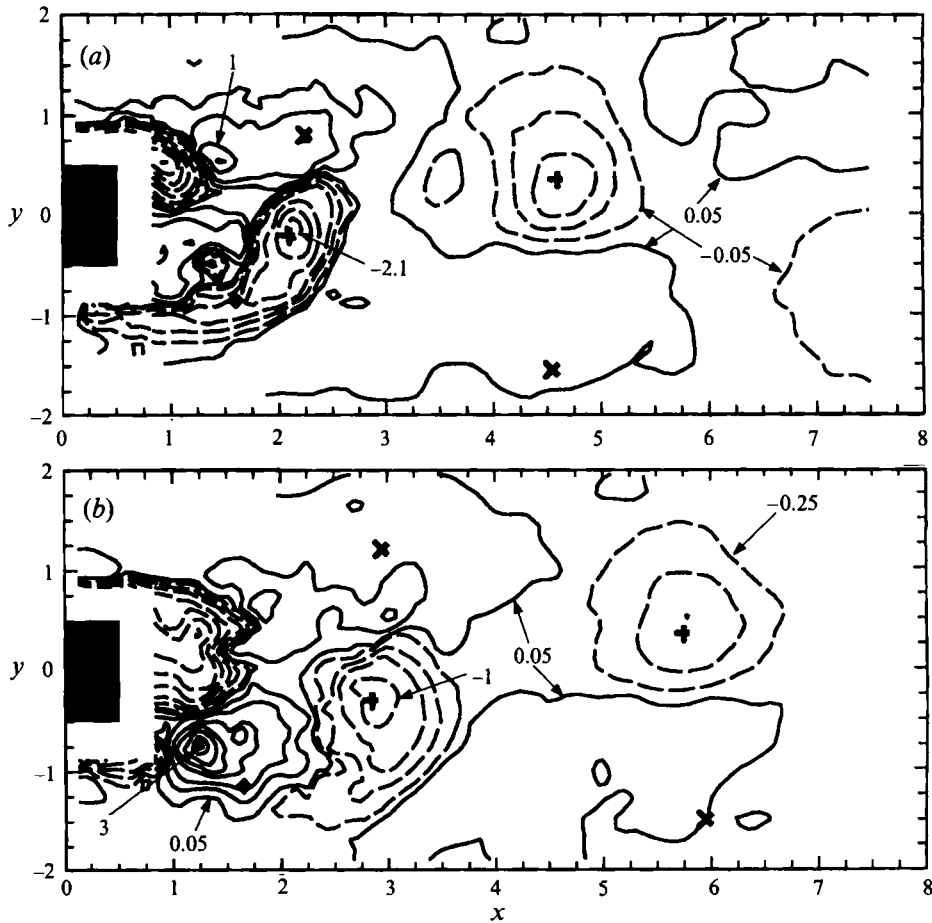


FIGURE 19. Contour plots of $\langle D \rangle$ for (a) phase (5,15), and (b) phase (9,19): contour levels $-\pm 0.05, \pm 0.25, \pm 0.5, \pm 1, \pm 1.5, \pm 2.1, \pm 2.7, \pm 3, \pm 3.6$.

The experimental work was performed at the Institut für Hydrodynamik, Universität Karlsruhe, and was financially supported by the German Research Foundation through the Sonderforschungsbereich 210. The last author (J.-H. P) would like to acknowledge the support of the Korea Science and Engineering Foundation. Discussions with Dr. E. Adams and Dr. V. Kolár were helpful at various stages of the study as were the comments by Dr. S. Szepessy and the anonymous reviewers on previous drafts. The experimental rig was constructed by Mr. D. Bierwirth.

Appendix. The critical points of a stream-function distribution

The critical points of a stream-function distribution, $\phi(x, y)$, are defined by the conditions that $\phi_x = 0$ and $\phi_y = 0$ simultaneously, where subscripts denote the partial derivative with respect to the subscripted variable. This is identical to the requirement that $u = 0$ and $v = 0$ given in discussions of flow topology. Whether a critical point, (x_0, y_0) , is a local extrema (centre) or a saddle depends on the sign of the discriminant, $D(x_0, y_0) \equiv [\phi_{xy}^2 - \phi_{xx}\phi_{yy}]|_{(x_0, y_0)}$. If $D(x_0, y_0) < 0$, then (x_0, y_0) is a local extrema, while if $D(x_0, y_0) > 0$, (x_0, y_0) is a saddle. If $D(x_0, y_0) = 0$, then higher-order terms must be considered to determine the nature of the critical point.

In terms of u and v , the discriminant can also be expressed as $D = (u_x)^2 + v_x u_y$, which is independent of reference frame velocity. An alternative approach which gives a similar criterion can be based on linearizing the flow in a localized region of the critical point (Perry & Fairlie 1974; Ottino 1989).

If $D < 0$ in a region, then, irrespective of the reference-frame velocity, a streamline saddle cannot be found in this region. Similarly, if $D > 0$ in a region, then a streamline saddle may be found, the location of which would depend on the choice of reference-frame velocity. At a point of zero vorticity, then $D = (u_x)^2 + (u_y)^2$, which is non-negative. Thus, a point of zero vorticity may be a saddle, provided it is also a stagnation point (in an appropriate reference-frame). Whether the choice of reference frame velocity which would make a zero-vorticity point also a stagnation point is a physically 'relevant' velocity, e.g. corresponding to vortex celerity, must however be considered. The contours of D (or in the present specific context, $\langle D \rangle$) are shown for phases (5,15) and (9,19) in figure 19. Regions of peak negative $\langle D \rangle$ correspond closely to regions of peak vorticity (figure 7a). The vorticity saddle at $(x, y) \approx (1.7, -0.9)$ is located in a region where $\langle D \rangle < 0$, implying that a streamline saddle cannot be found at the vorticity saddle. Although some error might be expected in both measurement and computation of gradients, the region of negative $\langle D \rangle$ is sufficiently extensive to make this inference fairly reliable. High levels of vorticity do not exclude the possibility of a streamline saddle. A positive- $\langle D \rangle$ region at phase (9,19) penetrates a region of high vorticity at $(x, y) \approx (1.6, -1)$, and a streamline saddle can indeed be found in the region (figure 6b).

REFERENCES

- BEARMAN, P. W. 1967 On vortex street wakes. *J. Fluid Mech.* **28**, 625–641.
- BEARMAN, P. W. 1969 On vortex shedding from a circular cylinder in the critical Reynolds number regime. *J. Fluid Mech.* **37**, 577–585.
- BEARMAN, P. W. & OBASAJU, E. D. 1982 An experimental study of pressure fluctuations on fixed and oscillating square-section cylinders. *J. Fluid Mech.* **119**, 297–321.
- BEARMAN, P. W. & TRUEMAN, D. M. 1972 An investigation of the flow around rectangular cylinders. *Aero. Q.* **23**, 229–237.
- CANTWELL, B. J. & COLES, D. 1983 An experimental study of entrainment and transport in the turbulent near wake of a circular cylinder. *J. Fluid Mech.* **135**, 321–374 (referred to herein as CC).
- COURCHESNE, J. & LANEVILLE, A. 1982 An experimental evaluation of drag coefficient for rectangular cylinders exposed to grid turbulence. *Trans ASME I: J. Fluids Engng* **104**, 523–527.
- DURAO, D. F. G., HEITOR, M. V. & PEREIRA, J. C. F. 1986 A laser anemometry study of separated flow around a squared obstacle. In *Laser Anemometry in Fluid Mechanics III* (ed. R. J. Adrian, et al.). LADOAN-IST, Lisbon, Portugal.
- DURAO, D. F. G., HEITOR, M. V. & PEREIRA, J. C. F. 1988 Measurements of turbulent and periodic flows around a square cross-section cylinder. *Exps. Fluids* **6**, 298–304.
- FAGE, A. & JOHANSEN, F. C. 1927 On the flow of air behind an inclined flat plate of infinite span. *Proc. R. Soc. Lond. A* **116**, 170–197.
- FAGE, A. & JOHANSEN, F. C. 1928 The structure of vortex sheets. *Phil. Mag. (7)* **5**, 417–441.
- GERRARD, J. H. 1966 The mechanics of the formation region of vortices behind bluff bodies. *J. Fluid Mech.* **25**, 401–413.
- HUSSAIN, A. K. M. F. 1983 Coherent structures – reality and myth. *Phys. Fluids* **26**, 2816–2850.
- HUSSAIN, A. K. M. F. 1986 Coherent structures and turbulence. *J. Fluid Mech.* **173**, 303–356.
- HUSSAIN, A. K. M. F. & HAYAKAWA, M. 1987 Eduction of large-scale organized structures in a turbulent plane wake. *J. Fluid Mech.* **180**, 193–229 (referred to herein as HH).
- HUSSAIN, A. K. M. F. & REYNOLDS, W. 1970 The mechanics of an organized wave in turbulent shear flow. *J. Fluid Mech.* **41**, 241–258.

- KÁRMÁN, T. VON 1912 Über den Mechanismus des Widerstandes, den ein bewegter Körper in einer Flüssigkeit erfährt. *Göttingen Nachr., Math.-Phys. Klasse*, pp. 547–556.
- KIYA, M. & MATSUMURA, M. 1988 Incoherent turbulence structure in the near wake of a normal plate. *J. Fluid Mech.* **190**, 343–356.
- LYN, D. A. 1992 Ensemble-averaged measurements in the turbulent near wake of a square cylinder: a guide to the data. Rep. CE-HSE-92-6. School of Civil Engng, Purdue University.
- LYN, D. A. & RODI, W. 1994 The flapping separated shear layer formed by flow separation from the forward corner of a square cylinder. *J. Fluid Mech.* **267**, 353–376.
- MCKILLOP, A. A. & DURST, F. 1986 A laser anemometry study of separated flow behind a circular cylinder. In *Laser Anemometry in Fluid Mechanics II* (ed. R. J. Adrian, et al.) LADOAN-IST, Lisbon, Portugal.
- NAKAMURA, Y. 1993 Bluff-body aerodynamics and turbulence. *J. Wind Engng Ind. Aero.* **49**, 65–78.
- NORBERG, C. 1993 Flow around rectangular cylinders: Pressure forces and wake frequencies. *J. Wind Engng Ind. Aero.* **49**, 187–196.
- OSHIMA, H. & RAMAPRIAN, B. R. 1991 The use of particle image velocimetry to study vortex shedding behind a cylinder. *Trans. ASME I: J. Fluids Engng* **108**, 15–20.
- Ottino, J. M. 1989 *The Kinematics of Mixing: Stretching, Chaos, and Transport*. Cambridge University Press.
- OWEN, F. K. & JOHNSON, D. A. 1980 Measurements of unsteady vortex flowfields. *AIAA J.* **18**, 1173–1179.
- PERRY, A. E., CHONG, M. S. & LIM, T. T. 1982 The vortex shedding process behind two-dimensional bodies. *J. Fluid Mech.* **116**, 77–90.
- PERRY, A. E. & FAIRLIE, B. D. 1974 Critical points in flow patterns. *Adv. Geophys. B* **18**, 299–315.
- PERRY, A. E. & STEINER, T. R. 1987 Large-scale vortex structures in turbulent wakes behind bluff bodies. Part 1. Vortex formation processes. *J. Fluid Mech.* **174**, 233–270.
- ROSHKO, A. 1954 On the drag and shedding frequency of two-dimensional bluff bodies. *NACA TN* 3169.
- TENNEKES, H. & LUMLEY, J. L. 1972 *A First Course in Turbulence*. MIT Press.
- TRIANAFYLLOU, G. S., TRIANAFYLLOU, M. S. & CHRYSOSTOMIDIS, C. 1986 On the formation of vortex streets behind stationary cylinders. *J. Fluid Mech.* **170**, 461–477.
- WEST, G. S. & APELT, C. J. 1982 The effects of tunnel blockage and aspect ratio on the mean flow past a circular cylinder with Reynolds number between 10^4 and 10^5 . *J. Fluid Mech.* **114**, 361–377.
- ZHOU, Y. & ANTONIA, R. A. 1994 Critical points in a turbulent near wake. *J. Fluid Mech.* **275**, 59–82.